EUROPEAN COMMISSION

Community Research

SEVENTH FRAMEWORK PROGRAMME

CARBOWASTE

Treatment and Disposal of Irradiated Graphite and Other Carbonaceous Waste

Grant Agreement Number: FP7-211333

Technical Report (WP3.Task 3.2)

Characterization before and after irradiation of EDF Saint-Laurent A2 reactor stack graphite

Author(s): L. Gosmain, J. Comte, S. Parraud, D. Cury, M. Sonnaert

Date of issue of this report : February 2012

Start date of project : **01/04/2008** Duration : **48 Months**

Project co-funded by the European Commission under the Seventh Framework Programme (2007 to 2011) of the European Atomic Energy Community (EURATOM) for nuclear research and training activities		
Dissemination Level		
PU	Public	
RE	Restricted to the partners of the CARBOWASTE project	
CO	Confidential, only for specific distribution list defined on this document	**X**

Distribution list

Person and organisation name and/or group	Comments
W. Von Lensa, CARBOWASTE Project coordinator	
G. PINA, Work Package 3 leader	
B. Grambow, Work Package 6 leader	
L. Petit, EDF	
S. Schumacher, ANDRA	
A. Jones, University of Manchester	
Ch. Lamouroux, CEA	
C. Ferry, CEA	
P. Thouvenot, CEA	
CARBOWASTE beneficiaries.	

CARBOWASTE		
Work package: 3 **Task: :** 3.2	**CARBOWASTE document no:** CARBOWASTE-1201-D-WP3.Task.2 (e.g. May 2008 as date of issue: 0805)	**Document type: T** D=Deliverable / M=Minutes / P=Progress report / T=Technical Report
Issued by: CEA **Internal no.:** Technical report CEA SL2 WP3		**Document status:** Final

Document title

Characterization before and after irradiation of EDF Saint-Laurent A2 reactor stack graphite

Executive summary

This document describes the characterizations performed on virgin [unirradiated] and irradiated graphite samples from the EDF Saint-Laurent A2 reactor. The aim of these analyses is to discover the physical properties of the graphites, properties which are essential to understanding the behaviour of graphite during reactor operation and of radionuclides in storage conditions.

The characterizations undertaken and reported here were carried out at DMN/SEMI/LPCMI and at DEC/SA3C/LARC in cooperation with DSN/SEEC/LECD, and relate to measurements of density, porosity and pore distribution, as well as characterizations by X-ray diffraction of virgin and irradiated graphite. Following some technical problems, the characterizations by Raman spectroscopy initially planned will be carried out during the second half of 2010.
Variations in these properties during irradiation in the Saint-Laurent A2 reactor will be discussed.

Revisions

Rev.	Date	Short description	Author	Internal Review	Task Leader	WP Leader
00	02/2012	First issue	Gosmain CEA	Poussard CEA 14.2.2012		PINA CIEMAT

TABLE OF CONTENT

1. INTRODUCTION

Due to its good mechanical, thermal and physical properties (especially a good moderating power with regard to neutrons), graphite was the material of choice for producing the first nuclear reactors, whether for military, research or power generating purposes (UNGG reactors in France or Magnox in the UK). In France, all the graphite moderated, gas cooled reactors have been shut down (3 CEA and 5 EDF UNGG reactors) and now not only pose the problem of dismantling these reactors, but also that of handling the "graphite waste".

As part of the studies into the storage of "graphite" waste originating from this reactor type, it is particularly necessary to obtain scientific data on the behaviour of the long-lived radionuclides ^{36}Cl and ^{14}C given their mobility in the geological medium and their long radioactive period. To do this, an R&D programme was suggested for studying and quantifying the release mechanisms of these radionuclides in water, as well as for studying the variation in the microstructure of graphite under irradiation. This is because the characteristics of graphite porosity are essential parameters which will broadly influence the physical and chemical processes that control the release of radionuclides to the solution.

With this in mind, samples from the G2 reactor have already been characterized at the *Laboratoire de caractérisations Physico-Chimiques des Matériaux Irradiés* (Laboratory for Physical and Chemical Characterization of Irradiated Materials) (DMN/SEMI/LPCMI) and at the *Laboratoire d'Analyses Chimiques et Radiochimiques* (Laboratory for Chemical and Radiochemical Analyses) (DEC/SA3C/LARC) with the support of the *Laboratoire d'Expertise et de Caractérisation Destructive* (Specialist Laboratory in Destructive Characterization) (DSN/SEEC/LECD) **[1]**. To complete this initial study, identical characterizations (density, porosimetry and X-ray diffraction) were carried out on graphite from the Saint-Laurent A2 reactor. The results of the characterizations conducted at DMN/SEMI/LPCMI, DEC/SA3C/LARC and DSN/SEEC/LECD form the subject of the present report.

The first part of this report presents a summary of the literature on the subject, the reasons for choosing samples and their preparation before characterization. Also described are the experimental techniques used in these characterizations.

The second part relates to measurements of geometric density, porosimetry by helium and bromobenzene pycnometry, mercury intrusion porosimetry and finally to X-ray diffraction analyses. It should be noted that Raman spectroscopy characterizations were also planned on these samples, but following some technical problems, these characterizations were postponed to the second half of 2010 and will be carried out on the ATALANTE Raman facility at the CEA Marcoule centre.

2. THE SAINT-LAURENT A2 REACTOR

The Saint-Laurent A2 reactor was commissioned in August 1971 and finally shut down on 25 May 1992. The pressure vessel of this reactor is built of prestressed concrete, which also acts as biological shielding. As in the case of the G2 reactor, the coolant is CO_2 which circulates from top to bottom at a pressure of 29 bar in the space between the graphite liners and the Mg-Zr alloy fuel cladding **[2]**. It has a thermal power of 1 700 MW, a gross electrical power of 530 MWe and a net electrical power in nominal operation of 515 MWe **[3]**. The thermal neutron flux (10^{-5} eV to 0.5 eV) in the central zone of the core and in the maximum flux plane is $3.12\ 10^{13}$ $n.cm^{-2}.s^{-1}$.

It should also be noted that this reactor was shut down between March 1980 and September 1982 following an incident which led to the melting of two fuel elements at the bottom of the F5 M19 C14 channel (loss of cooling of the channel as a result of its obstruction by a metal plate, leading to overheating of the fuel elements) **[4]**.

2.1 THE STACK GRAPHITE

The graphite stack of the SLA2 reactor takes the form of a right cylinder with a vertical axis 15.73 metres in diameter (13.43 metres of moderator surrounded by a 1.15 m thick reflector) and 10.2 metres in height **(Figure 1)**. The total mass of graphite is 2 440 metric tons including 1 580 metric tons of moderator and 860 metric tons of reflector.

The stack's network of graphite bricks is a hexagonal mesh with a pitch of 225.16 mm. The elementary graphite blocks are prismatic bars with a hexagonal base whose distance between two opposite faces is equivalent to the network mesh. The side-by-side juxtaposition of 4 429 bars forms a bed, the SLA2 stack consisting of 8 superimposed beds (bed No. 1 is that at the bottom of the stack). Thus, the bars are superimposed and the stack may also be regarded as the juxtaposition of 4 429 columns. The graphite stack comprises:

- The lateral reflector, consisting only of 828 solid columns surrounding the core,
- The moderator (or core) consisting of 3 601 columns: 345 solid columns, 181 bored to 84 mm for the control rods and 3 075 columns bored to 140 mm (basically for the fuel elements) **[5]**, **(Figure 2)**.

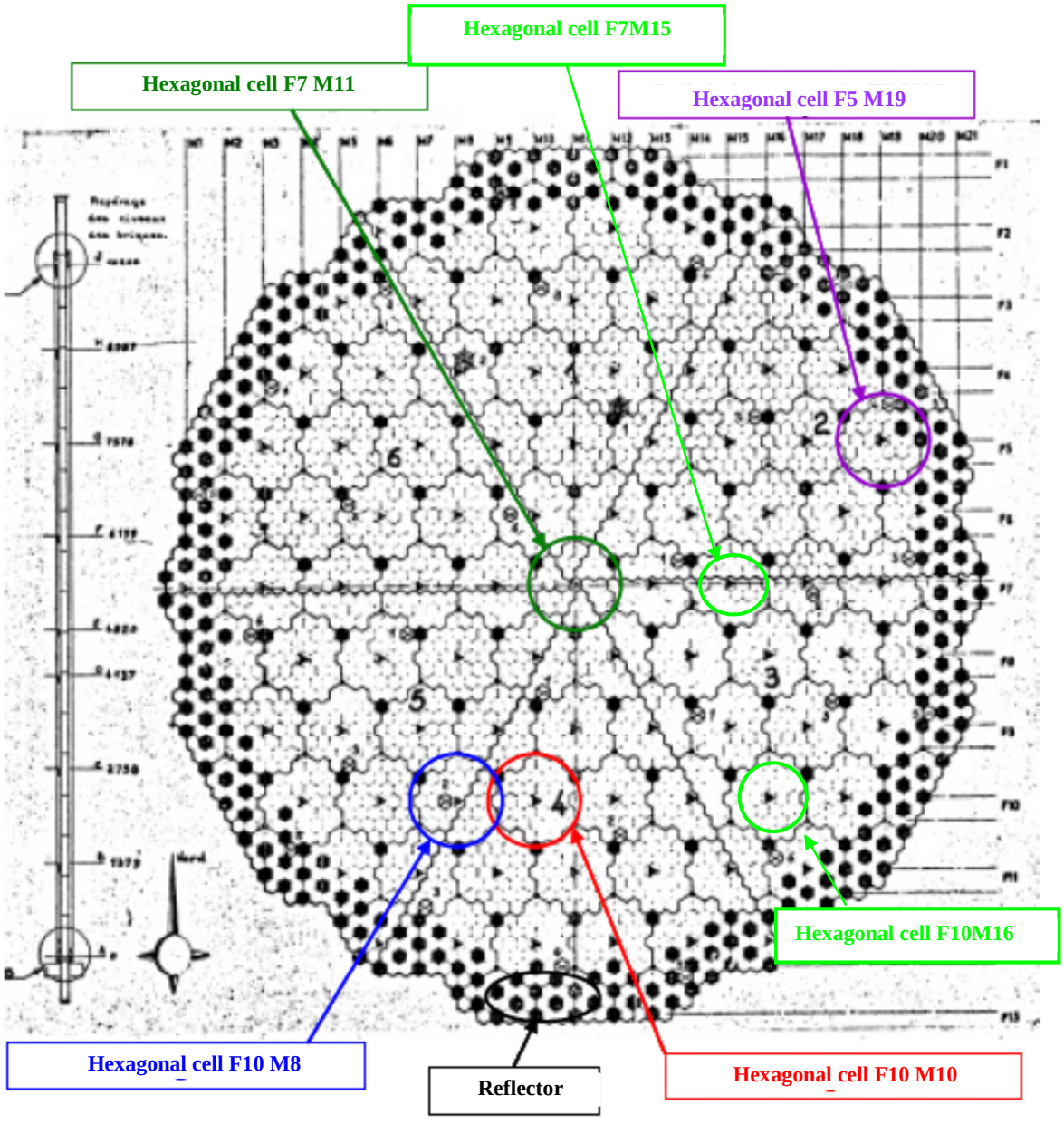

Figure 1: Section through the graphite stack of the Saint-Laurent A2 reactor

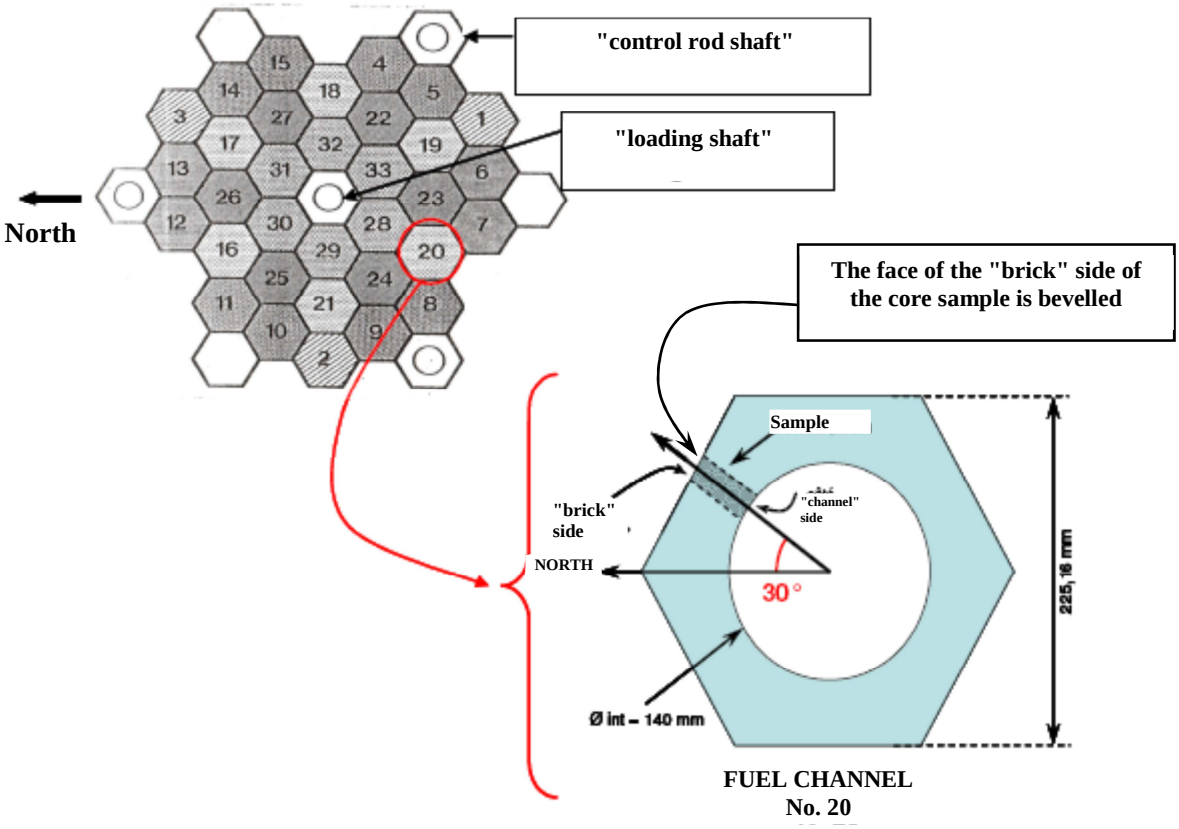

Figure 2: Schematic view of a hexagonal cell.

The graphite of the Saint-Laurent A2 stack was manufactured by the Pechniney/SERS company between May 1966 and November 1967. This graphite was made from Lima coke, underwent impregnation and was purified using MgF_2. During its manufacture it was tested particularly with regard to effective cross-sections, density measurements and other properties (chemical analyses, thermal expansion coefficients, mechanical strength, etc.). The document "*Caractéristiques du graphite de l'empilement St Laurent A2*" (Characteristics of the St Laurent A2 stack graphite) **[6]** covers the main elements measured over 164 operations of the production campaign, a summary of which is shown in **Table 1**.

Coke	MgF_2 purified Lima coke
Bulk density	1.68
Capture section	3.75 mbarn
Ash content	98.2 ppm
Coefficient of thermal expansion $\alpha(\perp)$	$3.81.10^{-6}$ C^{-1}
Coefficient of thermal expansion $\alpha(//)$	$2.41.10^{-6}$ C^{-1}
Anisotropy ratio $\alpha(\perp) / \alpha(//)$	1.6
Compressive strength	42 MPa

Table 1: Main characteristics of SLA2 non-irradiated graphite obtained between 1966 and 1968 **[6]**.

Studies were also carried out on the porous texture of virgin graphites, in particular on simply impregnated LIMA coke based graphite **[7]** identical to the graphite of the St Laurent A2 stack. The results show that the simply impregnated LIMA coke based graphite displayed a density of 1.68 with a total porosity of 25.95% of which 22.88% is accessible to Hg (open porosity) and 3.07% not accessible (closed porosity). The porosity spectrum depicted in **Figure 3** shows porosity peaks at 20 µm, 2 µm and 0.02 µm.

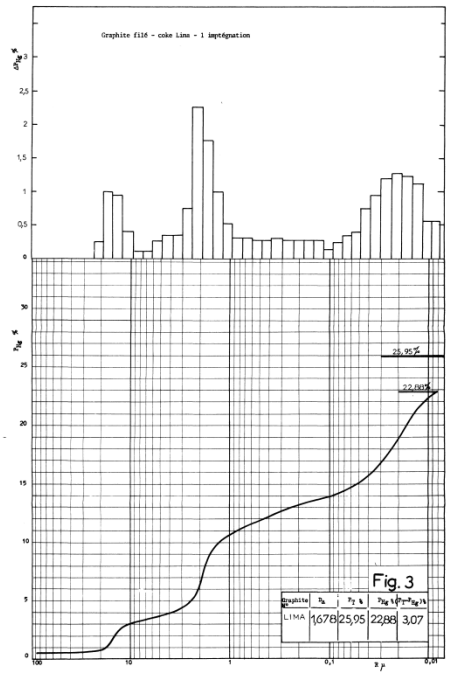

Figure 3: Mercury porosity spectrum of a once impregnated LIMA coke based graphite identical to the SLA2 stack graphite **[7]**.

2.2 DATA ACQUIRED ON SLA2 IRRADIATED GRAPHITE

The Saint-Laurent A2 reactor stack was subjected to core drilling in 2005 during which 180 cores were extracted. Several of these cores were used in order to conduct:

- physical characterizations at DMN/SEMI/LM2E and at DSN/SEEC/LECD (density, mechanical strength, etc.) **[5], [8]**,
- radiochemical characterizations carried out at DEC/SA3C/LARC at Cadarache or at DPC/SECR/LANIE at Saclay,
- and leaching tests during the dismantling that is currently in progress at CEA Cadarache for studying contamination transfer during decommissioning operations under water of the St Laurent A2 reactor.

A summary of the published data relating to geometrical densities is shown in **Table 2** and **Table 3**.

Height of sampling	*Geo. density*	*Wear* *Ref d = 1.684*	*Total porosity* d_{theo} = 2.266	*Open porosity (bromobenzene)*	*Closed porosity*
9260	1.666	1.05%	26.46%	21.69%	4.77%
8660	1.634	2.98%	27.90%	23.97%	3.93%
8270	1.615	4.11%	28.74%	24.33%	4.41%
6890	1.578	6.32%	30.38%	26.76%	3.62%
5120	1.559	7.45%	31.22%	26.42%	4.81%
4480	1.553	4.79%	31.48%	28.08%	3.40%
3450	1.600	5.00%	29.40%	25.83%	3.57%
2460	1.630	3.24%	28.09%	24.49%	3.60%
1680	1.590	5.56%	29.81%	24.48%	5.33%
300	1.733	-2.89%	23.53%	18.19%	5.34%
Average	***1.603***	***4.50%***	***29.28%***	***25.12%***	***4.16%***

Table 2: Porosity and density of samples from channel F10M10 − C20 of the SLA2 reactor **[5]**.

Height of sampling	Geo. density	Wear Ref d = 1.684	Pycnometry density He (+/-0.25%)	Total porosity d_{theo} = 2.266	Open porosity		Closed porosity
					(He)	(Hg)	
9260	1.65	2.0%	2.12	25.9%	22.4%	22.3%	3.7%
8660	1.64	2.6%	2.15	26.3%	23.7%	23.5%	2.6%
7280			2.15				
5510			2.14				
5120			2.15				
3450			2.14				
3060	1.60	5.0%	2.14	28.1%	25.3%	n.m	2.9%
2460	1.62	3.8%	2.12	27.2%	23.7%	24.4%	3.7%
2070	1.61	4.4%	2.10	27.7%	23.5%	21.8%	4.4%
1680	1.59	5.6%	2.11	28.6%	24.8%	22.9%	3.9%
300	1.68	0.2%	2.13	24.5%	21.1%	22.4%	3.4%
Average	**1.63**	**3.37%**	**2.13**	**26.90%**	**23.50%**	**22.88 %**	**3.51%**

Table 3: Porosity and density of samples from channel F5M19 − C20 of the SLA2 reactor **[8]**. The mercury porosity spectra obtained from the samples from channel F5M19 − C20 **[8]**, and shown in **Figure 4**, chiefly reveal three classes of pores: a zone of quite wide pores, between 3 and 100 nm, a second around a peak at 2-3 µm and lastly a zone located around 20 µm.

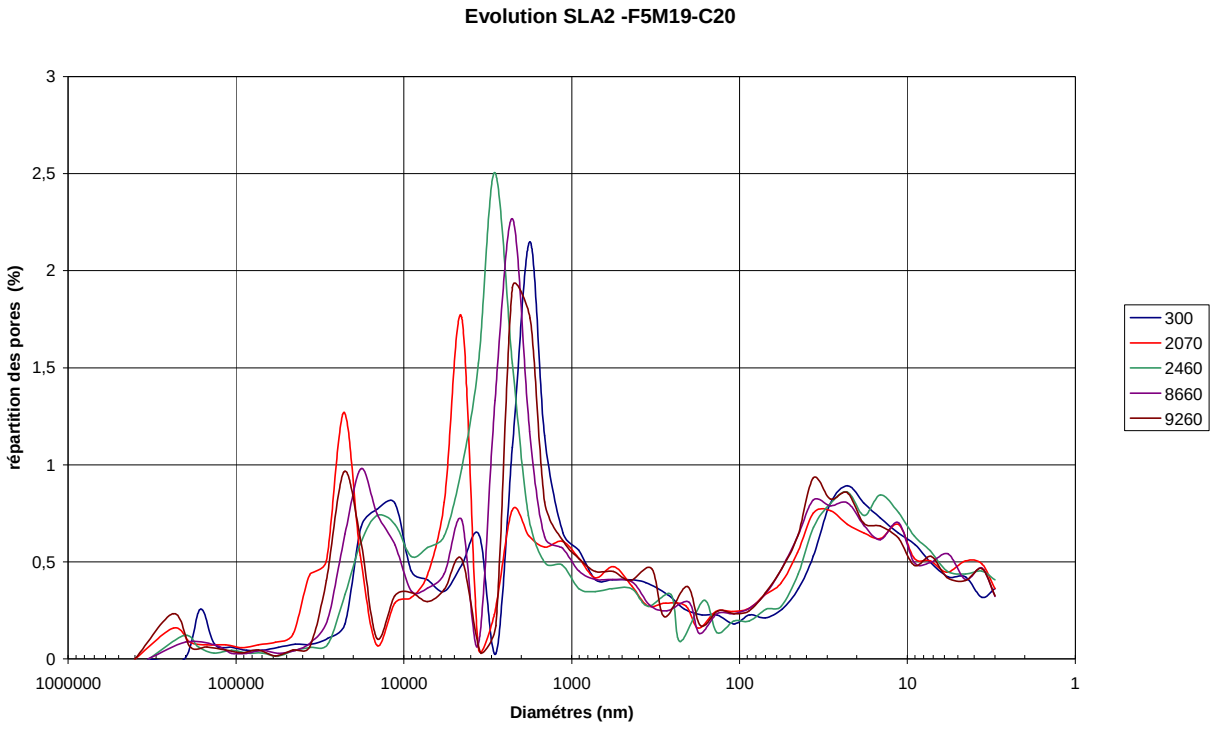

Figure 4: Mercury porosity spectra obtained from active SLA2 samples taken from channel F5M19-C20 **[8]**.

3. SELECTION AND PREPARATION OF SAMPLES

Within the context of studying the behaviour of radionuclides in irradiated graphites in an aqueous medium, two different reactors were studied, G2 and SLA2. These reactors were chosen based on the different characteristics of the stack graphite and the operating conditions of the reactors, in particular:

- nature of the coke and initial impurities,
- neutron and thermal powers, CO_2 pressure, thermal history of the graphite during reactor operation, presence of carboxyhydrogenated deposits.

Table 4 recalls the main differences between the reactors G2 and SLA2. It should be noted that this choice is also justified by the fact that a sufficient quantity of non-irradiated and irradiated graphite samples is available whose thermal and neutron history is fully known.

Reactor	***G2***	***SLA2***
Date of divergence	July 1958	June 1971
Date of shutdown	February 1980	May 1992
Thermal power (MW)	260	1700
CO_2 pressure (MPa)	1.5	28.5
Mass of graphite stack (m.t.)	1500	2200
Temperature of the graphite during operation	140 -380°C	240 -470°C
Nature of the graphite (core)	Grade A "special" coke	$MgFe_2$ purified Lima coke
Carbon deposits	"Low"	"High"
Graphite density	1.71	1.68

Table 4: Characteristics of reactors G2 and SLA2.

3.1 SLA2 REACTOR SAMPLES CHARACTERIZED AT DMN/SEMI/LPCMI

The SLA2 graphite samples available at LARC in the UNGG sample collection, and preselected within the context of the CT3 for leaching tests, originate from two different channels F10M16-C20 and F7M15-C19 located respectively at 5 m and 2.95 m radiuses from the centre of the reactor **(Figure 5)** and sampled at varying height levels. Three samples were selected per channel and sent to DMN/SEMI/LPCMI for structural characterizations **(Figure 6)**.

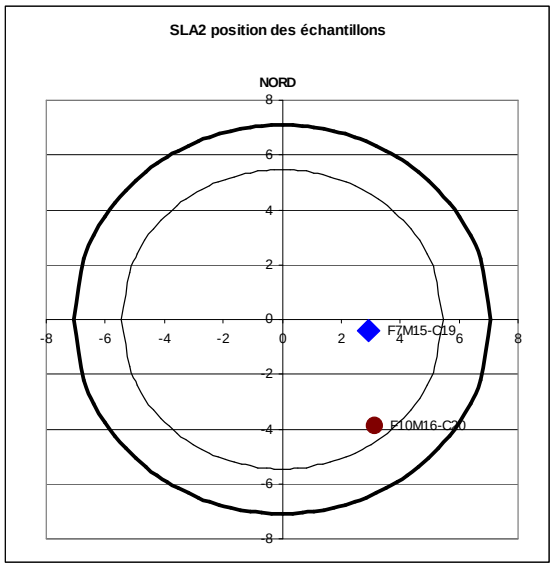

Figure 5: Position of channels F7M15 − C19 and F10M16 − C20 from which the samples characterized by LPCMI and LARC were taken.

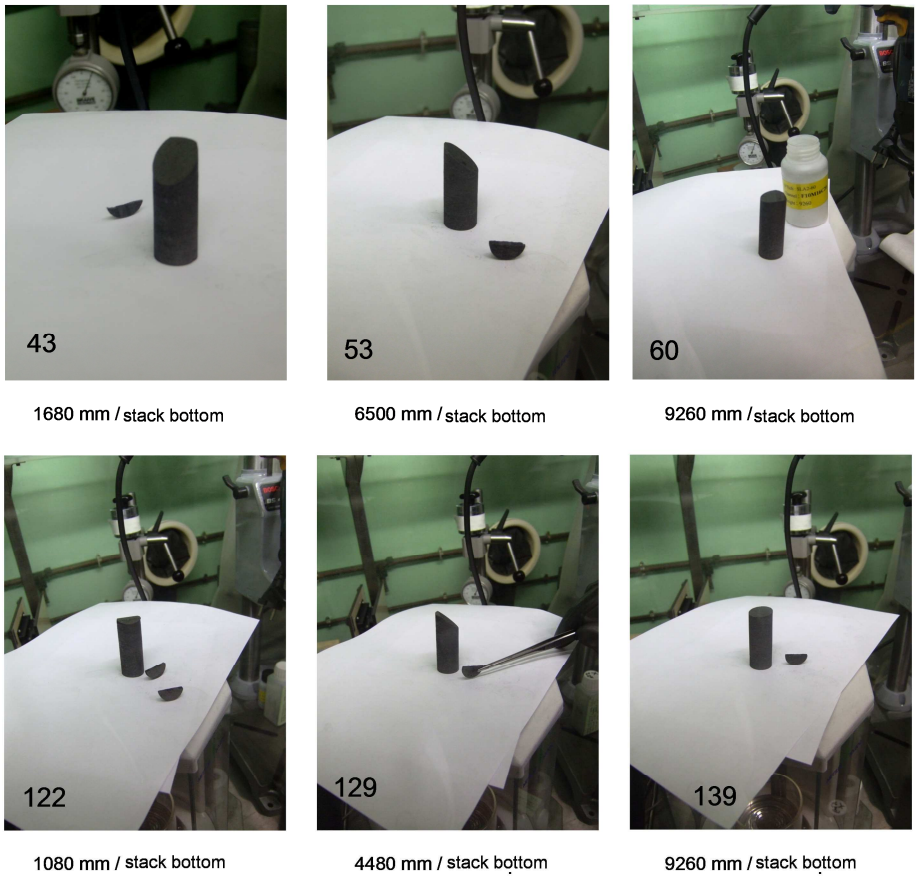

Figure 6: SLA2 graphite samples received at DMN/SEMI/LPCMI.

The information relating to taking these samples is shown in **Table 5**.

Channel	Elevation (mm)	Sample No.	Thermal history (°C)	Fast fluence E>0.1 MeV ($n.cm^{-2}$) (1)
F10M16 – C20	1680	SLA2-43	402	~ $2.0.10^{21}$
F10M16 – C20	6500	SLA2-53	282	~ $3.0.10^{21}$
F10M16 – C20	9260	SLA2-60	236	~ $1.4.10^{21}$
F7M15 – C19	1080	SLA2-122	412	~ $1.5.10^{21}$
F7M15 – C19	4480	SLA2-129	337	~ $3.3.10^{21}$
F7M15 – C19	9260	SLA2-139	236	~ $1.4.10^{21}$

(1) values calculated based on data from [5].

Table 5: Graphite samples characterized at DMN/SEMI/LPCMI.

Initially the samples were in the form of cylindrical cores with a bevelled end corresponding to the outer face of the brick **(Figure 2)**, and with the following approximate dimensions: diameter 19 mm / height 50 mm. In order to perform the geometrical and hydrostatic density measurements, as well as the X-ray diffraction analyses, it was necessary to re-machine the samples. The diagram in **Figure 7** summarizes the division of the samples for the various analyses to be carried out.

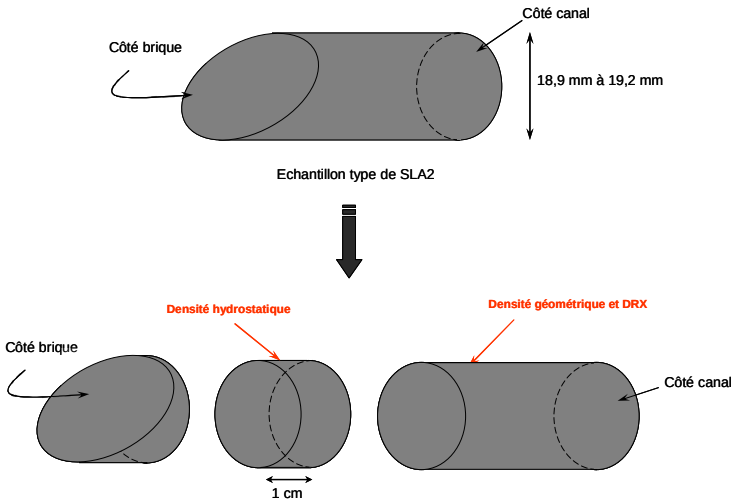

Figure 7: Schematic representation of an SLA2 graphite core and its division for the different analyses carried out at DMN/SEMI/LPCMI.

3.2 SLA2 REACTOR SAMPLES CHARACTERIZED AT DEC/SA3C/LARC

The samples characterized by LARC originate from the same channels as those sent to DMN/SEMI/LPCMI, but were taken from different elevations. These samples are intended for structural characterization, but also for carrying out leaching tests. The information relating to taking these samples is shown in **Table 6**.

Channel	*Elevation (mm)*	*Sample No.*	*Thermal history (°C)*	*Fast fluence E>0.1 MeV (n.cm^{-2}) (1)*
F10M16 – C20	2070	SLA2-44	435	~ 2.3.10^{21}
F10M16 – C20	7280	SLA2-55	310	~ 2.8.10^{21}
F10M16 – C20	8660	SLA2-58	270	~ 1.9.10^{21}
F7M15 – C19	2070	SLA2-124	455	~ 2.3.10^{21}
F7M15 – C19	7280	SLA2-135	310	~ 2.8.10^{21}
F7M15 – C19	8660	SLA2-138	270	~ 1.9.10^{21}

(1) values calculated based on data from [5].

Table 6: Graphite samples characterized at DEC/SA3C/LARC.

Initially the samples were in the form of cylindrical cores whose approximate dimensions are as follows: diameter 19 mm and height 50 mm. Cuts were then made in order to conduct the various characterizations. The six semi-circular samples selected for the leaching tests, were used first for determining initial activity in ^{36}Cl and secondly for porosity measurements (helium pycnometry and mercury porosimetry). The remainder of the core (approximately 40 mm in height) was planned for water immersion tests on a balance. The diagram in **Figure 8** summarizes the division of the samples for the various analyses to be carried out.

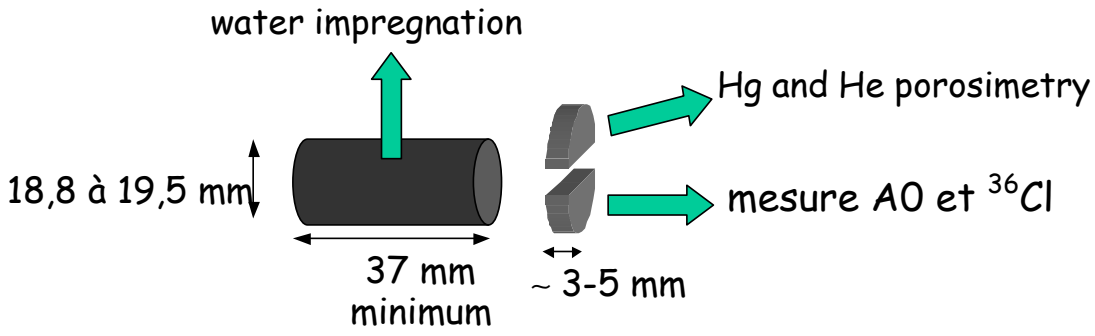

Figure 8: Schematic representation of an SLA2 graphite core and its division for the different analyses carried out at DEC/SA3C/LARC.

4. DESCRIPTION OF THE CHARACTERIZATION MEANS

In order to understand the phenomenon of radionuclide release during leaching tests on irradiated graphite and to study the changes in its microstructure, it is necessary to characterize the initial samples. For this, measurements of geometric and hydrostatic density with bromobenzene, helium pycnometry, mercury porosimetry and X-ray diffraction characterizations were carried out on active and inactive samples from the SLA2 reactor. These measurements were performed at DMN/SEMI/LPCMI at Saclay and at DEC/SA3/LARC in cooperation with DSN/SEEC/LECD at Cadarache.

4.1 DENSITY MEASUREMENTS

The geometric density measurements were obtained:
- by measuring the dimensions of the samples with a slide caliper (uncertainties 0.1 mm) taking several readings per dimension
- by weighing using precision balances.

4.2 HELIUM PYCNOMETRY

Pycnometry by displacement of helium is a technique for measuring the internal volume of a porous material and deducing its density from its mass. The measurement principle is based on the properties of helium, which behaves as a perfect gas. Some helium is placed under pressure in a reference chamber of known volume, then the sample chamber of known volume under atmospheric pressure is opened. Changes in pressure are related to the porosity of the sample. The gas fills the open porosity of the sample, only the dense fraction and closed porosity of the sample is not accessible. It is a non-destructive technique. The cells used enabled measurements to be carried out on samples of the order of one gram to about ten grams.

4.3 MERCURY POROSIMETRY

Mercury intrusion porosimetry is a technique that can be used to determine the pore size distribution of a porous, massive or powdery material. It is a destructive technique. The measurement principle is based on the properties of a non-wetting liquid at ambient temperature such as mercury. The mercury must be forced to penetrate the pores of a porous material. The intrusion pressure P that has to be applied to mercury so that it penetrates into a pore of diameter d is given by the Laplace equation (1):

$$P = \frac{4\gamma \cos\theta}{d} \quad (1)$$

where: P: intrusion pressure of mercury (Pa)
γ: surface tension of mercury (Pa/m)
θ: wetting angle of mercury on the surface of the pores (°)
d: diameter of the pores (m).

The pressure applied to the mercury is increased by increments and the volumes of mercury penetrating into the porous solid are recorded at each increment. The cumulative pore volume is then obtained as a function of the intrusion pressure or the diameter of the pores. The derivative gives the pore distribution of the solid. Knowing the density of the solid, the total quantity of mercury introduced into the solid can be used to determine the total porosity.
This method of study has some drawbacks. In particular, the high pressure (of the order of 400 MPa) applied to the mercury for it to penetrate the finest pores (a few nanometres in diameter) may alter the material studied. For this reason, the main usefulness of this technique is in displaying the distribution of pore size.
The use of Laplace's law amounts to considering all the pores as cylinders which is far removed from reality. Moreover, it must be assumed that the only sensitive factor is the diameter of the pore entrances. But significant hysteresis phenomena may conceal the actual pore structure. However, this technique is very useful for comparing different materials and forms a conventional representation of pore structure.

4.4 HYDROSTATIC DENSITY WITH BROMOBENZENE

The principle of measuring the hydrostatic density of a body is based on Archimedes principle. It consists of two weighings, the first being performed in air and the second in bromobenzene.

The real mass (*Mr*) of a sample is equal to its apparent mass to which must be added Archimedes thrust. The two weighings, in air and in bromobenzene, enable the following equality to be obtained (2):

$$Mr = M_1 + (Ve.\ \rho_a) = M_2 + (Ve.\ \rho_b) \quad (2)$$

where:

Mr: real mass of the sample (g)
M_1: mass of the sample weighed in air (g)
M_2: mass of the sample weighed in bromobenzene (g)
ρ_a: density of air ($g.cm^{-3}$)
ρ_b: density of bromobenzene ($g.cm^{-3}$)
Ve: geometric volume of the sample (cm^3). In this case, the sample is weighed in bromobenzene, but the bromobenzene does not wet the sample.

The geometric volume (*Ve*) of the sample can therefore be calculated by the relationship (3):

$$Ve = \frac{M_1 - M_2}{\rho_b - \rho_a} \quad (3)$$

The geometric density of the sample (ρ_g) can thus be deduced:

$$\rho_g = \left[\frac{M_1\left[\rho_b - \rho_a\right]}{M_1 - M_2}\right] + \rho_a \quad (4)$$

If, before immersing the sample in bromobenzene for weighing it, it is subjected to a primary vacuum, then the bromobenzene will imbibe all the open porosity of the sample **(Figure 9)**. A mass M_3 can therefore be defined: mass of the sample weighed in bromobenzene after imbibition.

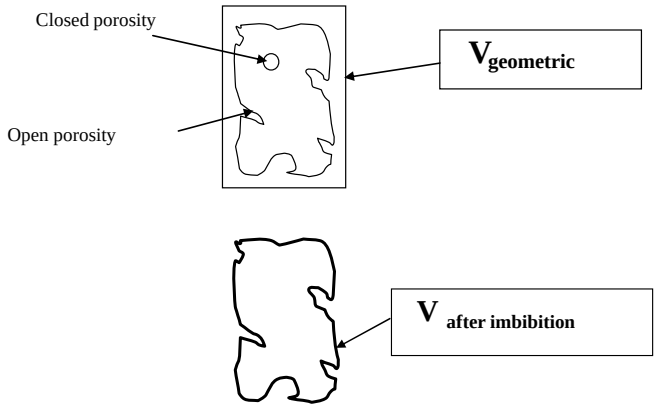

Figure 9: Geometric volume (V_e) and volume after imbibition ($V_e - V_{p0}$).

The two weighings in bromobenzene, before and after imbibition, enable the equality (5) to be obtained:

$$Mr = M_2 + (Ve.\ \rho_b) = M_3 + (Ve - Vpo)\ \rho_b \quad (5)$$

With *Vpo*: volume of open porosity.

The open porosity volume (*Vpo)* of the sample can therefore be calculated by the relationship (6):

$$Vpo = \frac{M_3 - M_2}{\rho_b} \quad (6)$$

The apparent or "skeletal" density of the sample (ρ_a) can thus be deduced:

$$\rho_a = \frac{Mr}{V_e - Vpo}$$

$$\rho_a = \left[\frac{M_3 \left[\rho_b - \rho_a\right] \rho_b}{\left[M_1 - M_3\right] \rho_b \ + \ \left[M_3 - M_2\right] \rho_a} \right] + \rho_b \quad (7)$$

4.5 EXPRESSION OF THE RESULTS

The porosity distribution calculations (total porosity, open and closed porosity) were performed according to the relationships shown below:

Total porosity (P_T) is:

$$P_T(\%) = 100\left(1 - \frac{\rho_G}{\rho_{th}}\right) \quad (8)$$

where ρ_{th} is the theoretical density of the graphite crystal (2.266 g/cm^3) and ρ_G is the measured geometric density.

Open porosity (P_O) is:

$$P_O(\%) = 100\left(1 - \frac{\rho_G}{\rho_a}\right) \quad (9)$$

where ρ_a is the apparent density determined by helium pycnometry or by hydrostatic measurement in bromobenzene.

Closed porosity (P_F) not accessible to helium is:

$$P_F = P_T - P_O \quad (10)$$

4.6 X-RAY DIFFRACTION

The apparatus used is a Siemens D500 "θ/2θ" diffractometer with copper anticathode (Cu Kα1 and Cu Kα2 radiation) installed in a shielded cell **(Figure 10)**. In order to collimate the X-ray beam, this apparatus is equipped with slots before and after the sample with the following optical layout: 0.3° slit / 0.3° slit / sample / 0.3° slit / Soller slits / 0.05° slit. In addition, for filtering out possible parasitic radiation, this apparatus is equipped with a rear graphite monochromator (filtering of copper K_β radiation and X and γ parasitic radiation).

Acquisitions consisted of phase recordings in "θ/2θ" mode (variable incidence) over an angular range varying from 20° to 90° (2θ). The diffractograms were recorded at 40 KV / 30 mA (X-ray generator), with a step of 0.02° and a count time of 10 seconds per step.

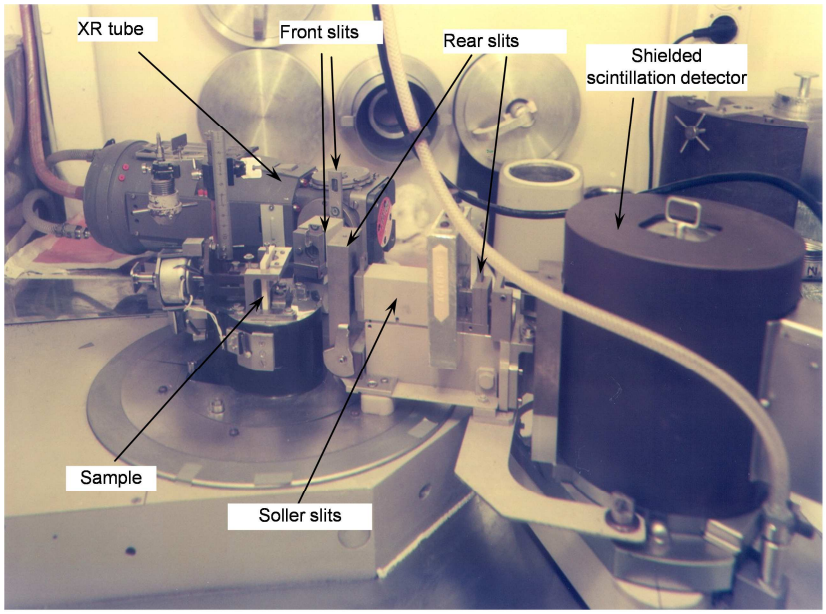

Figure 10: X-ray diffractometer in shielded cell (DMN/SEMI/LPCMI).

5. CHARACTERIZATION OF VIRGIN GRAPHITE FROM THE SLA2 REACTOR

The characterizations of Saint-Laurent A2 non-irradiated graphite were carried out on samples in the form of a cylinder approximately 8 cm long with a diameter of about 1.2 cm. These were core samples taken from once impregnated LIMA coke based graphite blocks (representative of SLA2 graphite) along two particular directions: parallel and perpendicular to the direction of extrusion of the graphite block.

5.1 GEOMETRIC DENSITY

The geometric density measurements on virgin graphite samples from the SLA2 reactor were carried out by three laboratories: DMN/SEMI/LPCMI, DEC/SA3C/LARC and DSN/SEEC/LECD. The results of these measurements are relatively consistent from one laboratory to another and are shown in **Table 7**.

The density measurements carried out on all the available samples (18 in total) lead to an average value of **1.69** ± **0.02** with values between 1.65 and 1.73, i.e. a dispersion of the order of 3% relative to the average. This density value leads to an estimate of the average total porosity of the characterized samples of **25.4 ± 1.3%**. These two values are perfectly consistent with the average values for density and total porosity previously obtained on graphite identical to that of the SLA2 reactor (once impregnated LIMA coke), values which are respectively **1.68** and **25.95% [6]**.

Sample No.	Direction of sampling	mass (g)	L (mm)	Ø (mm)	Geo. density	Total porosity (%)
3784-CD-38869	XY	15.208	80.00	12.00	**1.68 +/- 0.02**	***25.8 +/- 0.9 %***
	Z	15.102	79.98	12.00	**1.67 +/- 0.02**	***26.4 +/- 0.9 %***
3824-CD-39207	XY	15.185	80.10	12.02	**1.67 +/- 0.02**	***26.2 +/- 0.9 %***
	Z	15.206	80.11	12.03	**1.67 +/- 0.02**	***26.3 +/- 0.9 %***
3784-CD-38866	XY	15.253	80.00	12.00	**1.686 +/- 0.004**	*25.6 +/- 0.1%*
	Z	15.152	80.00	12.10	**1.647 +/- 0.004**	*27.3 +/- 0.1%*
3784-CD-38867	XY	2.394	12.40	12.00	**1.707 +/- 0.017**	*24.7 +/- 0.1%*
	Z	12.468	64.30	11.90	**1.734 +/- 0.005**	*23.5 +/- 0.1%*
3784-CD-38870	XY	15.523	80.00	12.00	**1.716 +/- 0.004**	*24.3 +/- 0.1%*
	Z	15.393	80.00	12.00	**1.701 +/- 0.004**	*24.9 +/- 0.1%*
3784-CD-38871	XY	15.547	80.00	12.00	**1.718 +/- 0.004**	*24.2 +/- 0.1%*
	Z	15.009	80.00	12.00	**1.659 +/- 0.004**	*26.8 +/- 0.1%*
3784-CD-38866	XY	2.797	14.42	11.99	**1.72 +/- 0.03**	*24.1%*
	Z	1.871	9.94	12.00	**1.67 +/- 0.03**	*26.5%*
3784-CD-38867	XY	2.828	14.61	11.99	**1.71 +/- 0.03**	*24.3%*
	Z	2.687	13.95	12.00	**1.70 +/- 0.03**	*24.8%*
3784-CD-38870	XY	2.803	14.55	11.99	**1.71 +/- 0.03**	*24.7%*
	Z	2.780	14.52	12.00	**1.69 +/- 0.03**	*25.2%*
Average value					***1.69 +/- 0.02***	***25.4 +/- 1.3%***

DMN/SEMI/LPCMI ( ), DEC/SA3C/LARC ( ), DSN/SEEC/LECD ( ).

Table 7: Geometric density and total porosity of virgin graphite from the SLA2 reactor.

5.2 DETERMINATION OF OPEN AND CLOSED POROSITY

Knowing the total porosity of a sample, there are two techniques that can be used for determining open and closed porosities: hydrostatic density measurements using bromobenzene with imbibition of the samples under vacuum (DMN/SEMI/LPCMI) and helium pycnometry measurements (DEC/SA3C/LARC and DSN/SEEC/LECD). Both techniques were used for the virgin samples from the SLA2 reactor and led to the results shown in **Table 8**.

It should be noted that since the measurements carried out at DEC/SA3C/LARC were conducted on samples with a small mass, the results obtained are tinged with considerable uncertainty and show a wide dispersion. Therefore they will not be included in the present study.

	Average geo. density	*Total porosity (%)*	*Hydrostatic density*	*Open porosity (%)*	*Closed porosity (%)*
3784-CD-38869 *Z*	**1.67 +/- 0.02**	**26.3 +/- 0.9**	**2.12 +/- 0.05**	**21.2**	**5.1**
3784-CD-38869 *XY*	**1.68 +/- 0.02**	**26.0 +/- 0.9**	**2.12 +/- 0.05**	**20.9**	**5.1**
LPCMI average	**1.67 +/- 0.02**	**26.2 +/- 0.9**	**2.12 +/- 0.05**	**21.1**	**5.1**
LECD average	**1.70 +/- 0.03**	**24.9**	**2.13**	**20.2**	**4.8**
Average value		**25.7 +/- 0.9**	**2.12 +/- 0.05**	**20.7**	**5.0**

Table 8: Total, open and closed porosities of virgin graphite from the SLA2 reactor.

The determinations of open and closed porosities are generally consistent and for the remaining interpretation of the results, we shall base ourselves on the average of the results obtained at DMN/SEMI/LPCMI and at DSN/SEEC/LECD: i.e. a total porosity of 25.7%, an open porosity of 20.7% and a closed porosity of 5.0%.

5.3 MERCURY POROSIMETRY

The mercury porosimetry measurements on virgin samples from the SLA2 reactor are currently in progress.

5.4 X-RAY DIFFRACTION

Two samples of non-irradiated graphite, representative of the Saint-Laurent A2 stack have been characterized at DMN/SEMI/LPCMI by X-ray diffraction in order to determine the lattice parameters *a* and *c* together with the mid-height width of the diffraction lines. The purpose of these determinations is to provide reference values which will be compared with the values obtained on irradiated samples and thus decide on the crystalline evolution of the SLA2 graphite under irradiation (possible swelling / deformation of the crystal lattice and changes in the size of the graphite crystallites).

Because of the anisotropic nature of graphite, due to its crystalline structure, also enhanced by the extrusion process, the two SLA2 samples characterized by XRD were taken in both main directions of the brick in order to reveal possible differences **(Figure 11)**: direction ⊥ to the extrusion (XY sample) and direction // to the extrusion (Z sample).

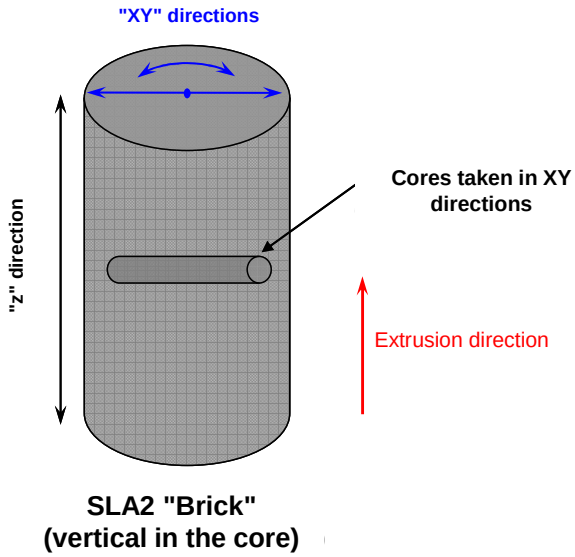

Figure 11: Sampling directions of virgin graphite samples from the SLA2 reactor stack.

The XRD readings are representative of ICDD data sheet No. 74-2330 relating to graphite **(Appendix 1)**. Enlargement of the area containing the main line for graphite − (002) − reveals a marked asymmetry of the diffraction lines for both samples characterized. Graphite is actually not a very dense material and the X-rays penetrate deeply into the interior of the samples, which causes an asymmetrical widening of the diffraction lines (absorption effect). The diffractograms obtained also reveal a weak crystallographic texture within the samples, a texture which is directly linked to the forming process by extrusion **(Figure 12)**. Which means there is an inversion of the intensity relations between line (002) and the other lines of the diffractogram. This rather unpronounced crystallographic texture is linked to the relatively low value of the anisotropy coefficient of the SLA2 graphite, around 1.6 as against 2.3 for the graphite of the G2 moderator for example (graphite which, on the other hand, displays a very marked crystallographic texture **[1]**.

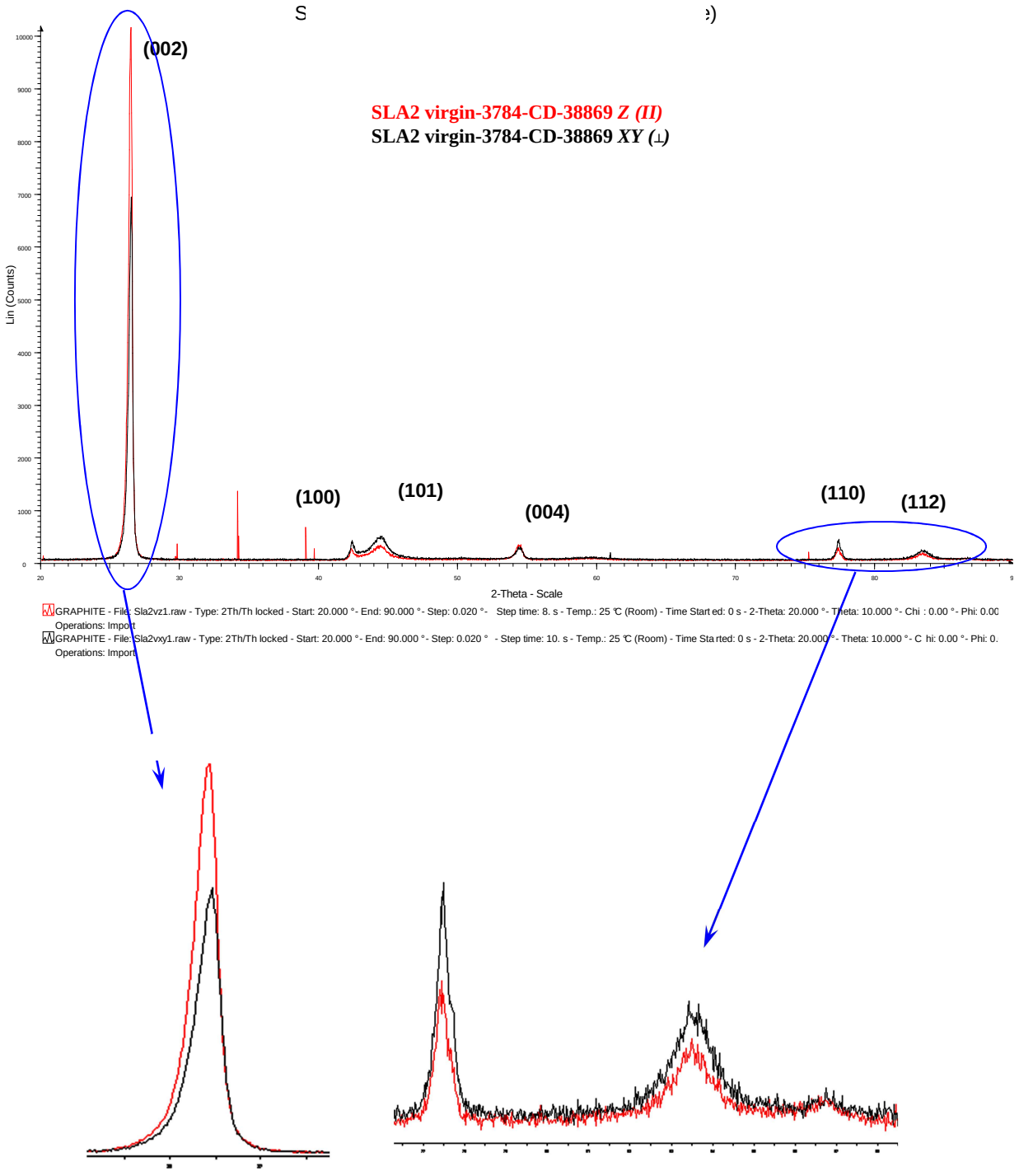

Figure 12: Diffractograms of virgin samples from the SLA2 reactor stack.

Analysis of the recorded diffractograms leads to the lattice parameters and diffraction line widths (002), (004) and (110) depicted in **Table 9** and **Table 10**.

SLA2	*Parameter c*	*Parameter a*
Theoretical parameters	***6.707***	***2.461***
3784-CD-38869 *XY (⊥)*	6.736	2.460
3784-CD-38869 *Z (//)*	6.740	2.462

Table 9: Lattice parameters of virgin graphite from the SLA2 reactor.

SLA2	*(hkl)*	*Position of lines (°)*	*Mid-height width (°)*
3784-CD-38869 *XY (⊥)*	002	26.418	0.306
	101	44.35	1.278
	004	54.439	0.602
	110	77.4715	0.371
3784-CD-38869 *Z (//)*	002	26.3875	0.305
	101	44.385	1.394
	004	54.4175	0.565
	110	77.4535	0.407

Table 10: Mid-height width of lines (002), (101) (004) and (110) of virgin graphite from the SLA2 reactor.

In the case of both samples, the values of parameter *a* are very close to the theoretical value, which means very good graphene plane structuring. Conversely, there is a significant difference in the values of parameter *c*. Since the distance between graphene planes is a very good indicator of the degree of graphitization of a graphite, this means in our case that the LIMA coke based graphite used for making the SLA2 reactor stack was not completely graphited (common for an industrial graphite). The establishment of a perfect three-dimensional structure for graphite in fact requires temperatures of more than 3 000°C whereas most manufacturing processes are content with 2 700 to 2 800°C.

The values of the diffraction line widths shown in **Table 9** do not call for any special comment; they will act simply as reference data which will be compared to the values obtained on the irradiated samples.

6. CHARACTERIZATION OF IRRADIATED GRAPHITE FROM THE SLA2 REACTOR

6.1 GEOMETRIC DENSITY

The geometric density measurements carried out at DMN/SEMI/LPCMI were conducted for samples Nos. 43, 53, 60, 122, 129 and 139 on pieces of samples intended for density and X-ray diffraction, but also on pieces of samples intended for hydrostatic density measurements **(Figure 7)**. The aim of these additional measurements was first to check whether the volume of matter characterized could have a significance for the result obtained, and secondly, to have geometric and hydrostatic density values for the same sample in order to calculate the percentage of total, open and closed porosities with the least possible error.

The results obtained on "large dimension" samples are shown in **Table 11**, those relating to samples of smaller dimensions are shown in **Table 12**. First to be noted is the fairly good reproducibility (apart from uncertainty) of the density values obtained on "large" and "small" dimensioned samples. In both cases, it appears that the geometric density of the samples decreases under irradiation, which is expressed in an increase in total porosity. This reduction in density is linked to wear of the graphite under irradiation (radiolytic corrosion). In the presence of pure CO_2, radiolytic corrosion occurs through the intermediary of active species formed by the radiolysis of carbon dioxide (CO_2) according to the following reactions:

$$\begin{cases} CO_2 + h\nu \rightarrow CO + O^* \\ O^* + C \rightarrow CO \end{cases}$$

Which taken together is equivalent to the Boudouard reaction:

$$CO_2 + C \rightarrow 2\ CO$$

Only the samples of core No. 60 show reverse development (increase in density compared with the non-irradiated reference of 1.69 ± 0.02). Since this development was not expected, a second series of measurements was undertaken on these samples, a new series which confirmed a high density value at this precise point. This finding can only be explained by the presence of local heterogeneities in density within the graphite brick in question, heterogeneities which have already been found for example in the graphite of the G2 reactor **[1]**. Local heterogeneities in density may be caused either by blowholes or lack of impregnation of the open porosity during the manufacture of the graphite (local drop in density), or on the contrary by the presence of zones very poor in porosity, e.g. due to dense agglomerations of coke grains. It must therefore be emphasized that the graphites used in the context of the UNGG [GCR] reactor type are materials that must be more regarded as "composite" (coke + binder + impregnant) than as homogeneous materials.

As a guide, **Table 13** shows the average of the density results obtained on the large and small dimensioned samples, results which lead to an average graphite wear of the order of 4.5% (a value identical to that obtained on channel F10M10-C20 **[5]**). Nevertheless, in further use of the density data, and especially in determining open and closed porosity values (next chapter), we shall adopt the geometric density values of the "small dimensioned" samples, i.e. those shown in **Table 12**. Since the geometric and hydrostatic density data are from the same samples, the determination of porosity levels will only be more reliable.

Sample	Elevation (mm)	T_{irr} (°C)	Mass (g)	Geo. density	Wear (%) (ref. to 1.69)	Total porosity (%)
F10M16-43	1680	402	21.9988	1.59 +/- 0.02	***5.65%***	***29.63%***
F10M16-53	6500	282	17.9422	1.60 +/- 0.02	***5.54%***	***29.55%***
F10M16-60	9260	236	22.1746	1.73 +/- 0.02	***- 2.17%***	***23.80%***
F10M16-60 2nd measurement			22.1746	1.72 +/- 0.02	***- 1.87%***	***24.02%***
F7M15-122	1080	412	22.0483	1.66 +/- 0.02	***1.87%***	***26.81%***
F7M15-129	4480	337	23.1589	1.56 +/- 0.02	***7.94%***	***31.34%***
F7M15-139	9260	236	22.0355	1.63 +/- 0.02	***3.84%***	***28.28%***

Table 11: Geometric densities of "large dimensioned" samples characterized at DMN/SEMI/LPCMI.

Sample	Elevation (mm)	T_{irr} (°C)	Mass (g)	Geo. density	Wear (%) (ref. to 1.69)	Total porosity (%)
F10M16-43	1680	402	4.6388	**1.58 +/- 0.02**	***6.48%***	***30.25%***
F10M16-53	6500	282	4.6989	**1.61 +/- 0.02**	***4.62%***	***28.87%***
F10M16-60	9260	236	5.0971	**1.73 +/- 0.02**	***- 2.37%***	***23.65%***
F7M15-122	1080	412	4.925	**1.67 +/- 0.02**	***1.13%***	***26.26%***
F7M15-129	4480	337	4.5661	**1.59 +/- 0.02**	***5.91%***	***29.83%***
F7M15-139	9260	236	4.8027	**1.63 +/- 0.02**	***3.57%***	***28.08%***

Table 12: Geometric densities of "small dimensioned" samples characterized at DMN/SEMI/LPCMI.

Sample	F10M16-43	F10M16-53	F10M16-60	F7M15-122	F7M15-129	F7M15-139
Geo. density	1.58 +/- 0.02	1.61 +/- 0.02	1.73 +/- 0.02	1.67 +/- 0.02	1.59 +/- 0.02	1.63 +/- 0.02
Wear (%) (ref. to 1.69)	6.27 %	4.86 %	- 2.30 %	1.32 %	6.42 %	3.64 %
Total porosity (%)	30.1 %	29.0 %	23.7 %	26.4 %	30.2 %	28.1 %

Table 13: Average of geometric densities of "large" and "small" dimensioned samples characterized at DMN/SEMI/LPCMI.

Table 14 summarizes the density results obtained at DEC/SA3C/LARC for the irradiated SLA2 graphite samples. It should be noted that since the core samples do not necessarily have parallel faces (slight slanting from being taken at the end of the brick depending on the orientation of the coring with respect to the outer face of the hexagonal brick − **Figure 2**) the geometric density values may be slightly distorted. To limit this effect, the geometric density measurements are supplemented by hydrostatic density measurements deduced after 64 days of water intake (without imbibition under vacuum).

The values obtained are generally comparable, save for uncertainties, to those obtained by DMN/SEMI/LPCMI, the small differences being able to be explained by the fact that the samples, while they may come from the same channel, have not been taken at the same elevation, and therefore have not been subjected to the same environmental conditions (neutron fluence, irradiation temperature). According to these results, the average wear found is of the order of 5.1% and is comparable with that estimated by DMN/SEMI/LPCMI.

Sample	Elevation (mm)	T_{irr} (°C)	Mass (g)	Average density	Total porosity (%)
F10M16-44	2070	435	21.9988	1.61 +/- 0.05	29.1 +/- 0.9
F10M16-55	7280	310	17.9422	1.62 +/- 0.04	28.6 +/- 0.8
F10M16-58	8660	270	22.1746	1.68 +/- 0.04	26.0 +/- 0.7
F7M15-124	2070	455	22.0483	1.55 +/- 0.05	31.5 +/- 1.1
F7M15-135	7280	310	23.1589	1.60 +/- 0.09	29.2 +/- 1.7
F7M15-138	8660	270	22.0355	1.56 +/- 0.12	31.0 +/- 2.4

Table 14: Geometric density of the irradiated graphite from the SLA2 reactor stack and characterized at DEC/SA3C/LARC.

The results obtained from shafts F10M16 and F7M15 match up well with the results obtained previously from shafts F10M10 and F5M19 **[5]**. This overall consistency of the density

measurements is further evidenced in **Figure 13**, which shows the variation in density, total porosity and wear of the graphite from the Saint-Laurent A2 stack depending on the axial position of the characterized samples. It appears that the loss of density of the graphite generally correlates with neutron fluence, the maximum flux plane of the Saint-Laurent A2 reactor being located at elevation 5 100 mm with respect to the bottom of the stack, a zone where the fall in density of the graphite is most marked.

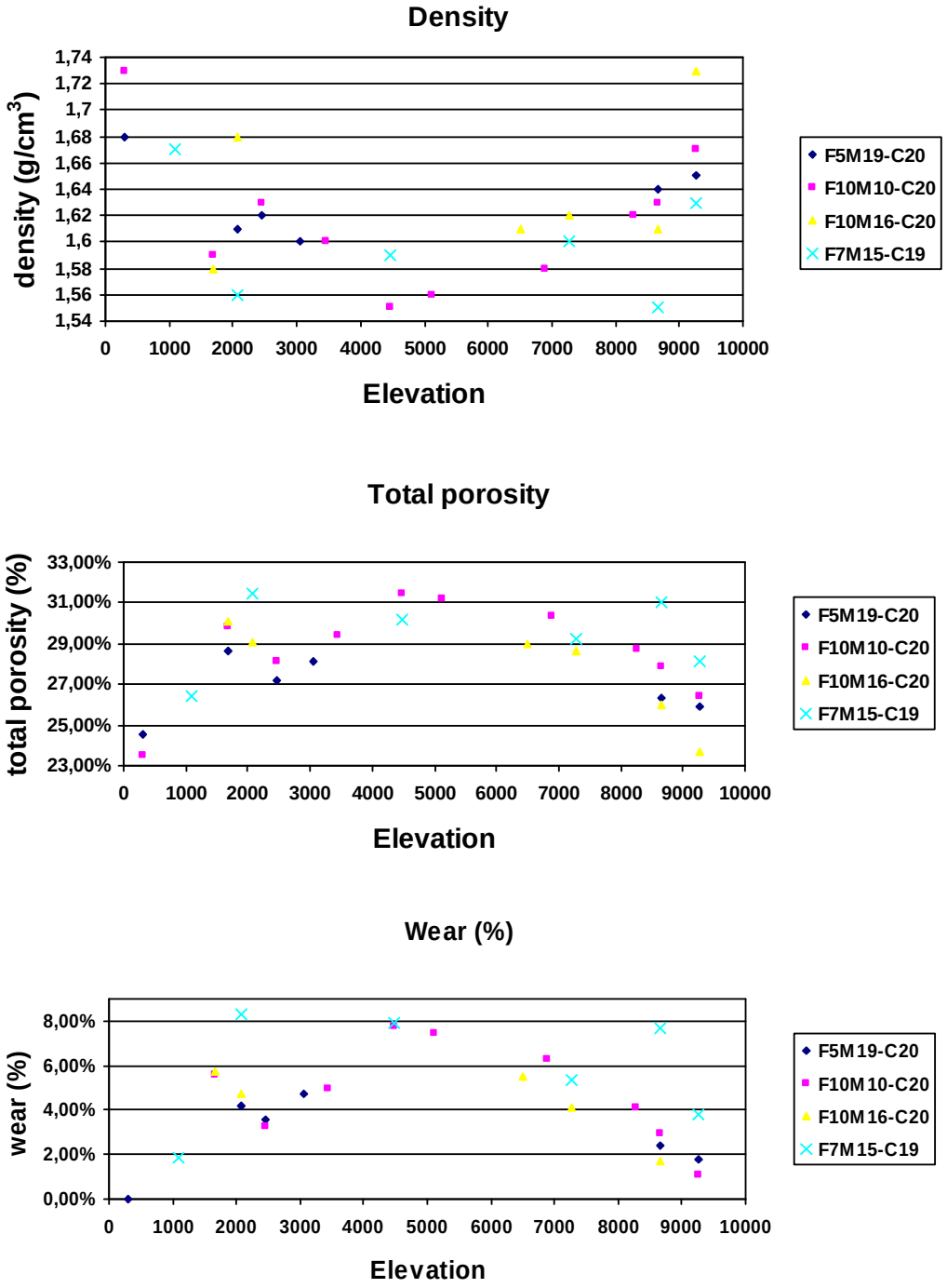

Figure 13: Variation in geometric density, total porosity and wear of the irradiated graphite samples according to their position in the SLA2 reactor.

It should be emphasized, however, that while the curves shown in **Figure 13** are relatively symmetrical with respect to the maximum flux plane (elevation 5 100 mm), they also display a discontinuity between elevations 1 500 mm and 2 000 mm with respect to the bottom of the stack, a discontinuity which could be explained by greater local wear. It should be noted that this discontinuity had also been revealed previously **[5]**. This discontinuity could be explained by two opposite competing phenomena when passing from the median plane of the reactor (elevation 5 100 mm) to the bottom of the stack: the increase in temperature encouraging radiolytic corrosion (since the coolant circulates from top to bottom of the stack, the graphite sees its temperature change from 240°C to about 400°C), and the fall in neutron fluence which causes the appearance of radical species O* which consume the graphite. The discontinuities in the density, total porosity and wear values between elevations 1 500 mm and 2 000 mm could thus be explained by the convolution of temperature and fluence effects, fluence then playing a predominant role with regard to the temperature of the coolant **(Figure 14)**. An alternative explanation could be that the neutron flux profile of the reactor is not symmetrical and locally displays more significant values thus leading to greater radiolytic corrosion.

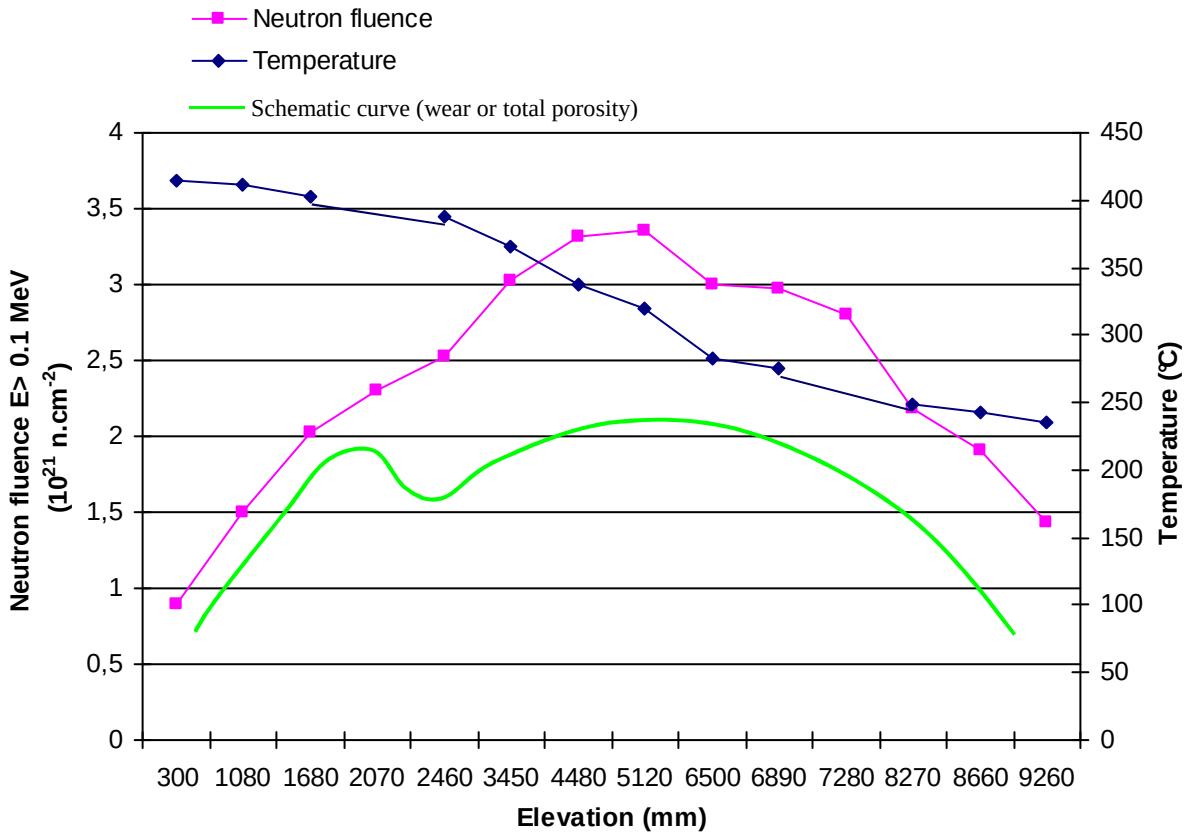

Figure 14: Axial variation in neutron fluence and temperature in the graphite stack of the SLA2 reactor and postulated schematic representation for wear.

6.2 OPEN AND CLOSED POROSITY VARIATION

As described previously (paragraph 3.2), and in the case of the characterizations carried out at DEC/SA3C/LARC, one of the ends of the SLA2 graphite cores was cut in a 10 mm thick, semi-circular shape for measuring striae **(Figure 8**). For each core, only one semi-circular disc was therefore used for helium and mercury porosity measurements. It should be noted that since the small mass of the sample was not conducive to the accuracy of the measurements, and taking into account the fact that there was only one piece per sample available (the rest of the core being used for geometric density measurements and for the leaching tests), no measurement reproducibility test was performed. It is therefore preferable to refer to the measurements from preceding campaigns (see reference **[5]**) and to the data from DMN/SEMI/LPCMI.

The characterization of open porosity and closed porosity was carried out at DMN/SEMI/LPCMI by conducting density measurements using bromobenzene with imbibition of the samples under vacuum. The results of these measurements are shown in **Table 15**.

Core	*Average geo. density*	*Total porosity (%)*	*Hydrostatic density*	*Open porosity (%)*	*Closed porosity (%)*	*T Irr (°C)*
Virgin	1.69 +/- 0.02	*26.2 +/- 0.9*	2.12 +/- 0.05	*21.2*	*5.1*	*NA*
F10 / M16 n°43	**1.58 +/- 0.02**	***30.2 +/- 0.9***	**2.11 +/- 0.05**	***25.1***	***5.2***	***402***
F10 / M16 n°53	**1.61 +/- 0.02**	***28.9 +/- 0.9***	**2.12 +/- 0.05**	***24.0***	***4.9***	***288***
F10 / M16 n°60	**1.73 +/- 0.02**	***23.7 +/- 0.9***	**2.09 +/- 0.05**	***17.2***	***6.4***	***236***
F7 / M15 - n°122	**1.67 +/- 0.02**	***26.3 +/- 0.9***	**2.12 +/- 0.05**	***21.2***	***5.1***	***412***
F7 / M15 - n°129	**1.59 +/- 0.02**	***29.8 +/- 0.9***	**2.13 +/- 0.05**	***25.4***	***4.5***	***337***
F7 / M15 - n°139	**1.63 +/- 0.02**	***28.1 +/- 0.9***	**2.12 +/- 0.05**	***23.1***	***4.9***	***236***

Table 15: Total, open and closed porosity values of irradiated graphite from the SLA2 reactor stack.

Apart from sample No. 60, the majority of the graphite samples see an increase in their total porosity due to radiolytic corrosion, resulting in a reduction in their density. The greater total porosity is associated with an increase in open porosity, but in contrast to the case of G2 **[1]**, the level of closed porosity remains constant (4.9% on average). It should be noted that while the open porosity values agree with the results previously obtained (shafts F10M10 and F5M19), the level of closed porosity seems a bit high, the average value obtained on shafts F10M10 and F5M19 being around 3.9%. In **Figure 15**, it appears that the open porosity level generally correlates with the neutron fluence received by the samples, and therefore with their axial position in the graphite stack, but it also shows the discontinuity already referred to previously between elevations 1 500 mm and 2 000 mm. On the other hand, it is harder to assess the variation in closed porosity according to the position of the samples in the core. In the light of these results, the decrease in density of the samples from the SLA2 reactor stack definitely stems from radiolytic corrosion of the graphite, this being all the greater the higher the neutron flux level and temperature, even though in principle the neutron fluence plays a predominant role.

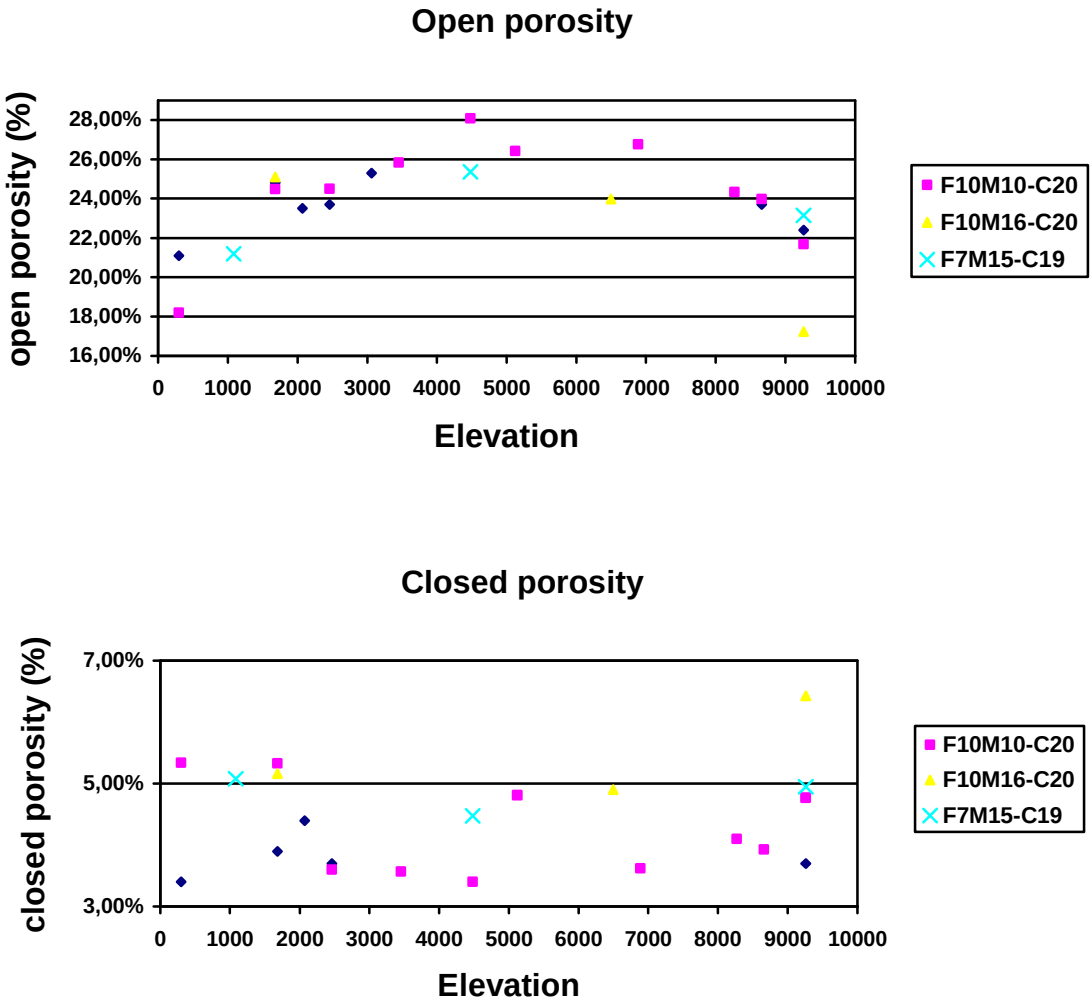

Figure 15: Variation in open porosity and closed porosity of the irradiated graphite samples according to their axial position in the Saint-Laurent A2 reactor stack.

6.3 MERCURY POROSIMETRY

As for the helium porosity measurements, only small quantities of graphite could be dedicated to the determination of porosities by mercury intrusion (see paragraph 6.2). Accordingly, the tests could not be duplicated. These tests were performed on the Hg porosimeter installed in a glove box at the Chicade facility. The variation in pore volume according to the diameter of the pores and the pore distribution of the samples from channel F10M16 and channel F7M15 are shown respectively in **Figures 16 and 17**, with **Figure 18** collecting the results together.

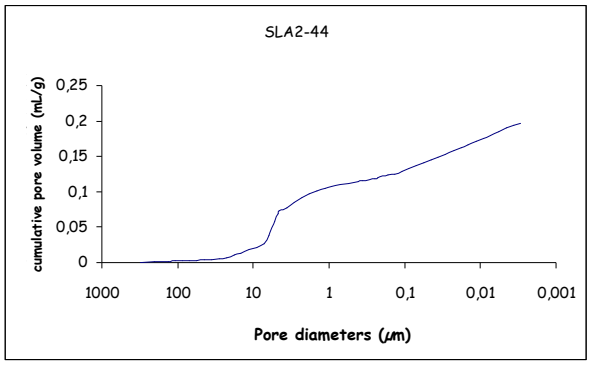

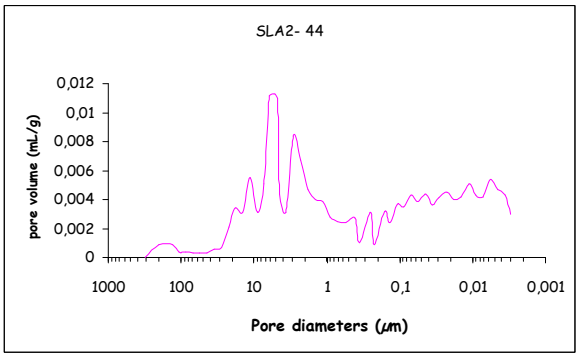

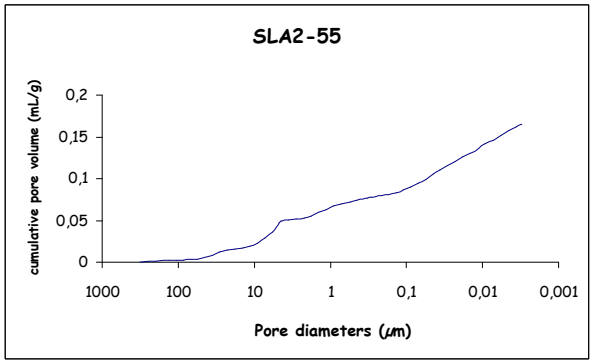

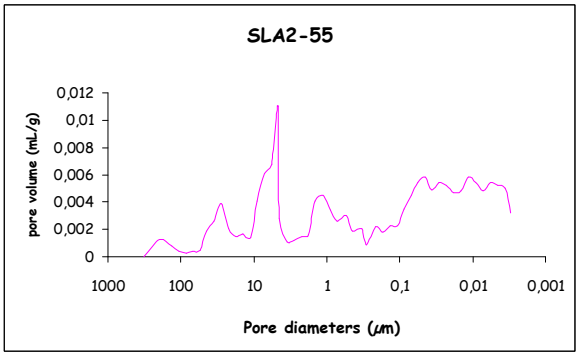

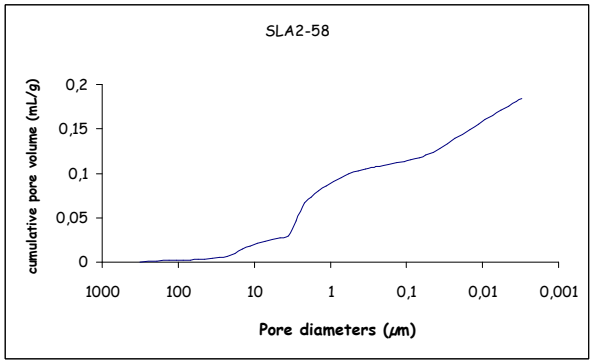

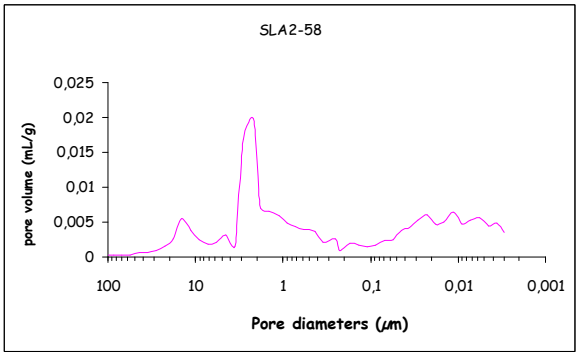

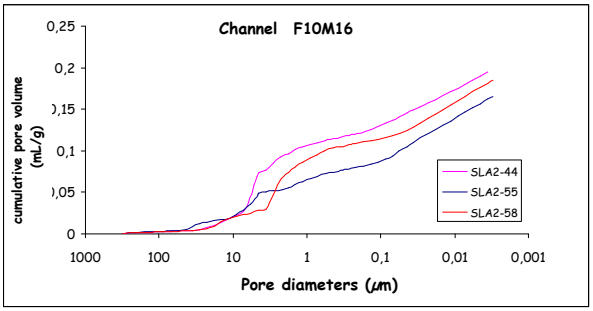

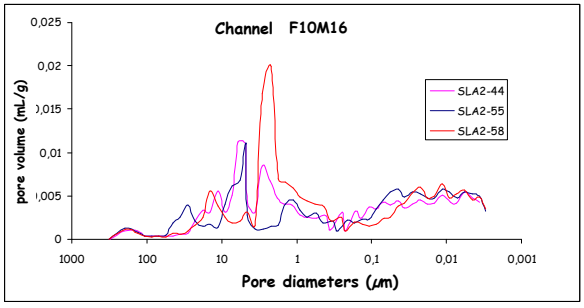

Figure 16: Mercury porosimetry spectra for the irradiated samples from channel F10M16-C20 of the SLA2 reactor.

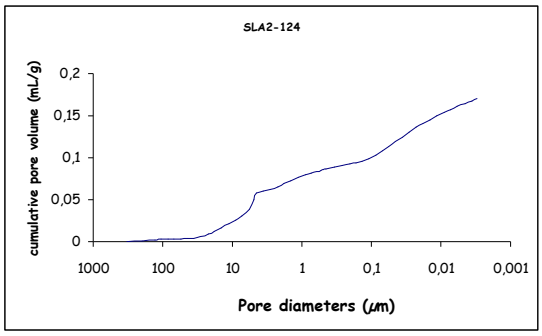

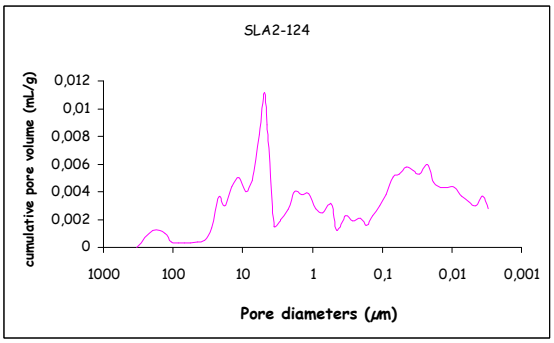

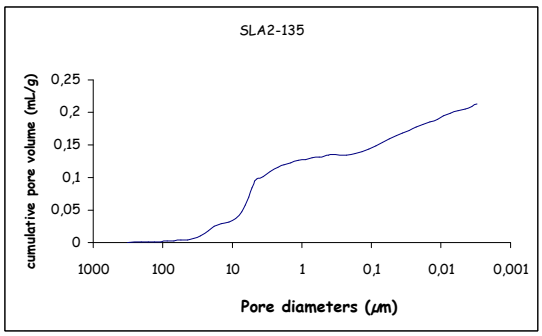

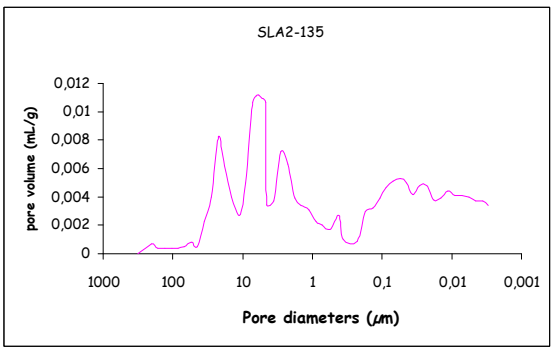

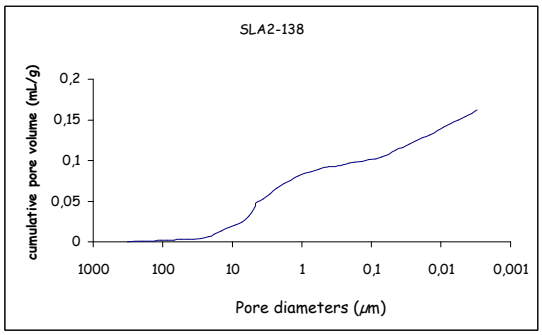

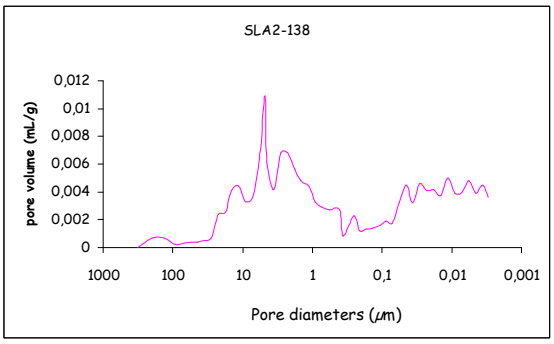

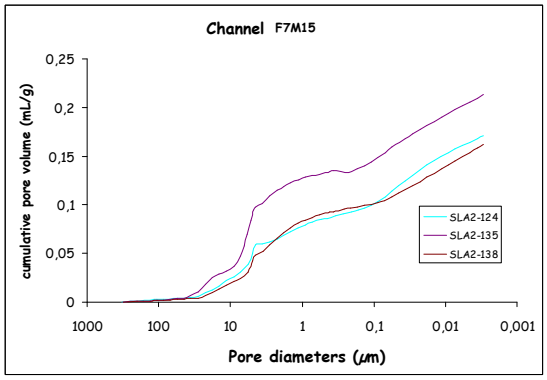

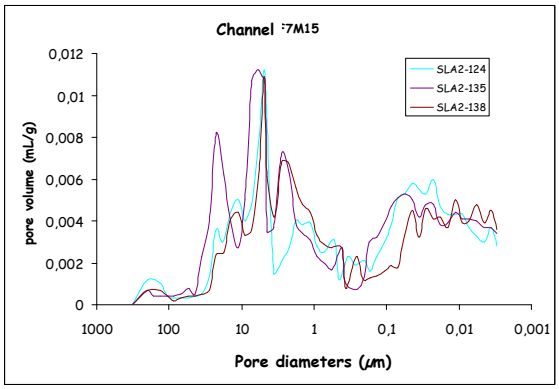

Figure 17: Mercury porosimetry spectra for the irradiated samples from channel F7M15-C19 of the SLA2 reactor.

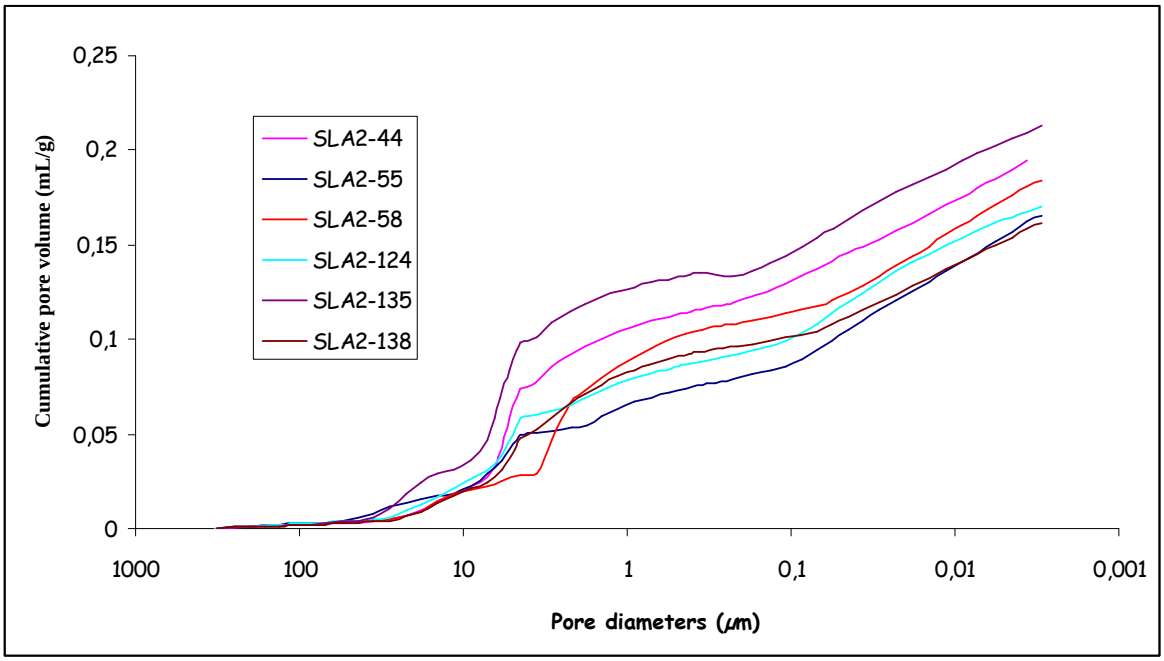

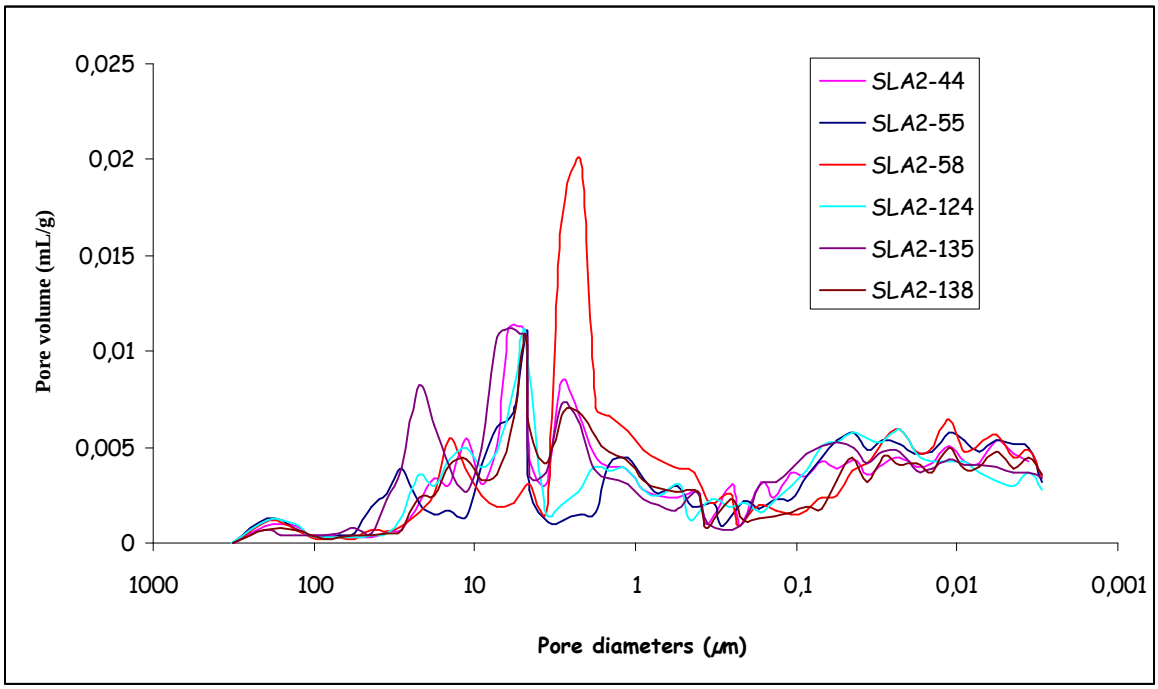

Figure 18: Mercury porosimetry spectra for the irradiated samples from channels F10M16-C20 and F7M15-C19 of the SLA2 reactor.

Overall it appears that all the active samples have a significant fraction of pores in the mesoporosity domain (pore diameter between 1 and 300 nm), and a peak in porosity at about the 3-5 µm size (especially in sample No. 58). Finally, there is a third porosity zone around 10 µm, but with a greater dispersion (varying from 8 to 20 µm) according to the samples.
In the absence of mercury porosimetry data for the SLA2 reactor virgin graphite, an analysis cannot be conducted on possible variation in the pore structure of SLA2 graphite during irradiation. The analysis of the data obtained from the various irradiated samples according to their position in the reactor stack does not allow any conclusions as to the impact of neutron flux or temperature on changes in the graphite's structure. Sample No. 58 from channel F10M16 does display a slightly different pore structure from that of the other samples, but it would be necessary to obtain new acquisitions in order to confirm these initial results.

6.4 X-RAY DIFFRACTION

Given the orientation of the different cores taken in channels F10M16-C20 and F7M15-C19 (perpendicular to the brick extrusion axis), the orientation of the irradiated samples characterized by X-ray diffraction is identical to that of virgin sample 3784-CD-38869 XY **(Figure 11)**. Therefore the data obtained will preferably be compared to those originating from the non-irradiated sample 3784-CD-38869 XY. The lattice parameters *a* and *c* and the mid-height width of the diffraction lines have been determined for these six irradiated samples.

As for the non-irradiated reference samples, the XRD readings are representative of ICDD data sheet No. 74-2330 relating to graphite **(Appendix 1)** and all the samples characterized display a significant asymmetry of the diffraction lines at low 2θ angles, especially for the main line (002) **(Figure 19)**. It will be recalled that this asymmetry is linked to the low density of graphite: since the X-rays penetrate deeply into the interior of the samples, this causes an asymmetrical widening of the diffraction lines (absorption effect). In this figure, it should also be noted that the line associated with the basal planes of the graphite crystal (002) shifts towards the low diffraction angles, which leads to an overall increase in parameter *c*. Conversely, the diffraction lines associated with the prismatic planes of the graphite crystal (100) and (110) shift towards the high diffraction angles, which leads to an overall decrease in parameter *a*.

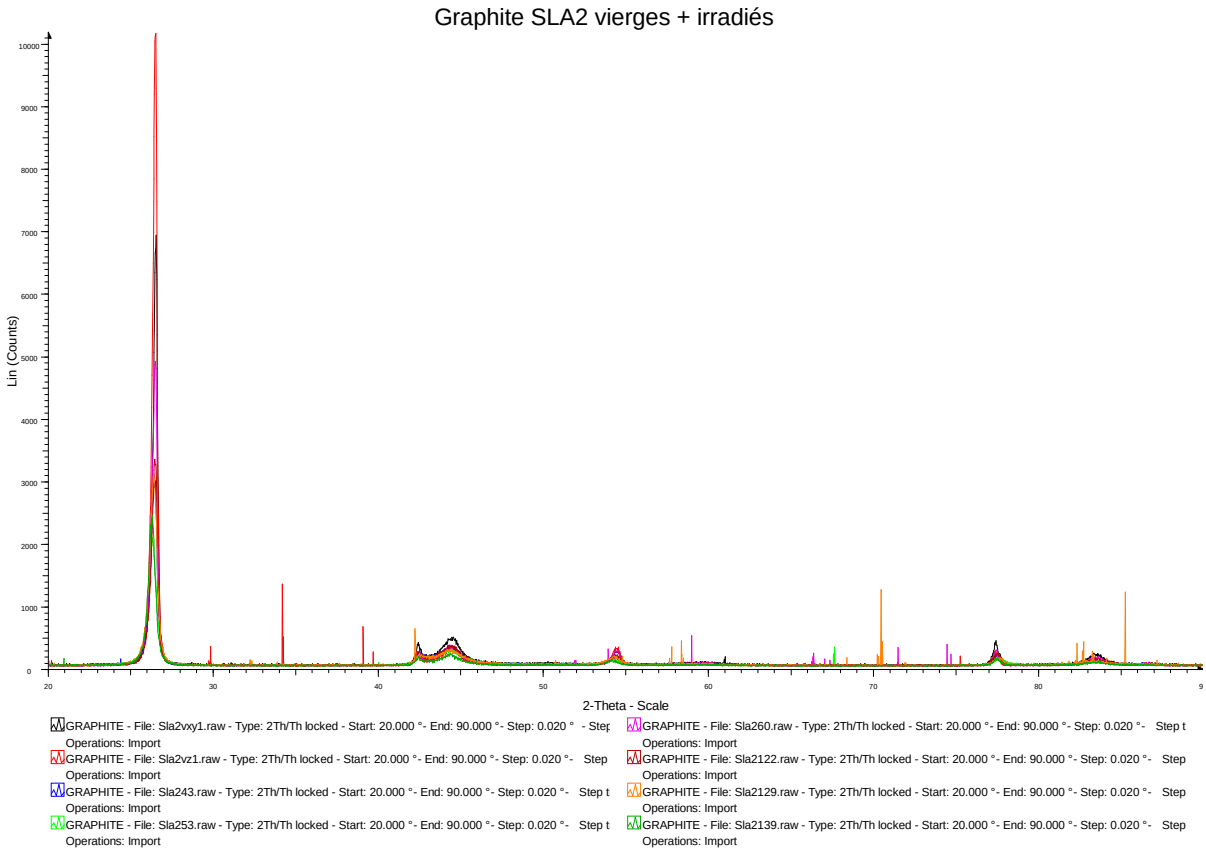

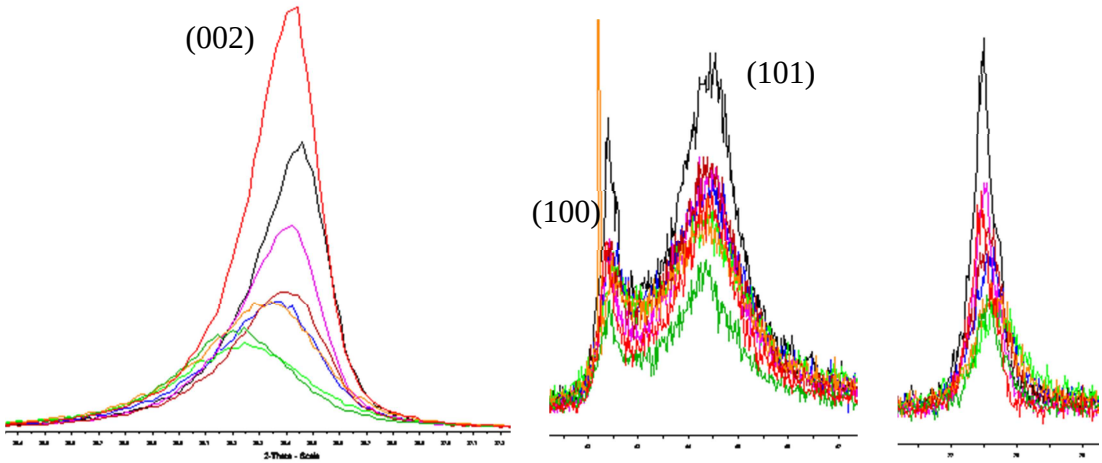

Figure 19: Diffractograms obtained from virgin and irradiated samples from the SLA2 reactor graphite stack.

The qualitative variations of the crystal parameters (decrease in *a* and increase in *c*) are consistent with the data in the literature **[9]**. These dimensional variations in the graphite crystallites are directly linked to defect creation/migration due to neutron irradiation. The neutrons displace carbon atoms in the graphite crystal which leads to the creation of carbon atoms in an interstitial position (increase in parameter *c*), and the creation of gaps within the graphene planes (decrease in parameter *a*): **Figure 20.** Since the force of the bonds between the graphene planes is much weaker than that inside the planes, the creation of irradiation defects leads to a much more significant variation in parameter *c* than parameter *a*.

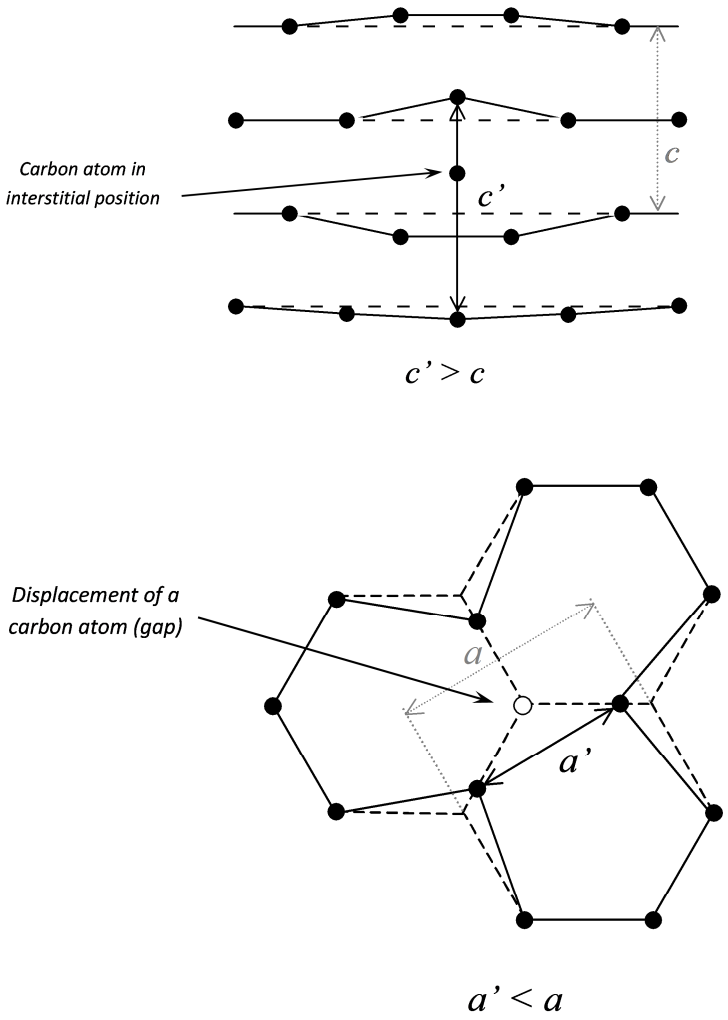

Figure 20: Changes in crystal parameters in the graphite linked to the presence of defects due to neutron irradiation.

The variation in crystal parameters is a function of the quantity of defects created, therefore of the neutron fluence and temperature of irradiation. The more the fluence increases, the more the parameters are modified up to a threshold value beyond which the defects will recombine and no longer participate in modifying the crystal parameters. In the same way, the higher the irradiation temperature, the more the defects will become mobile and be prone to recombine, leading to a lesser effect on the variation in crystal parameters **(Figure 21)**.

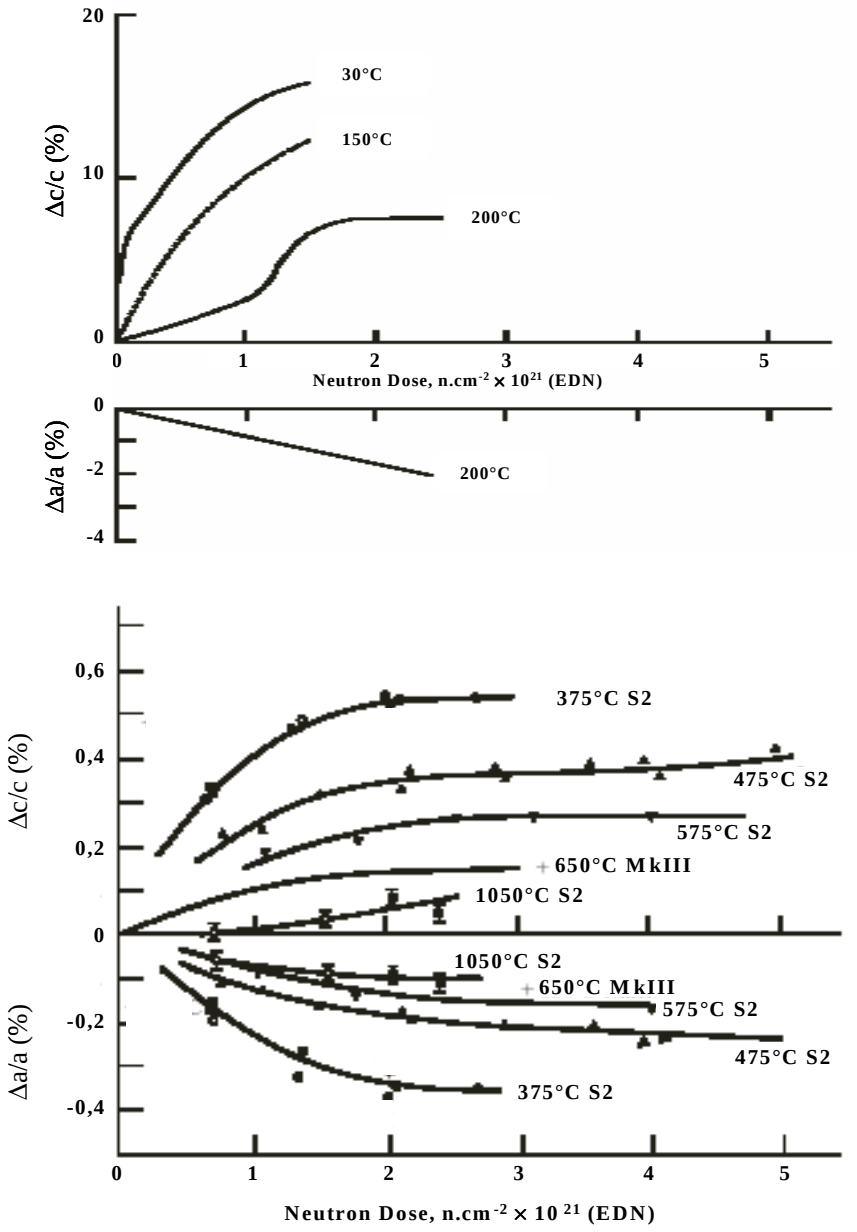

Figure 21: Changes in crystal parameters of graphite as a function of neutron fluence and irradiation temperature, according to **[11]**.

Figure 22 shows the diffractograms obtained on reference sample 3784-CD-38869 XY and the irradiated samples from shaft F10M16.

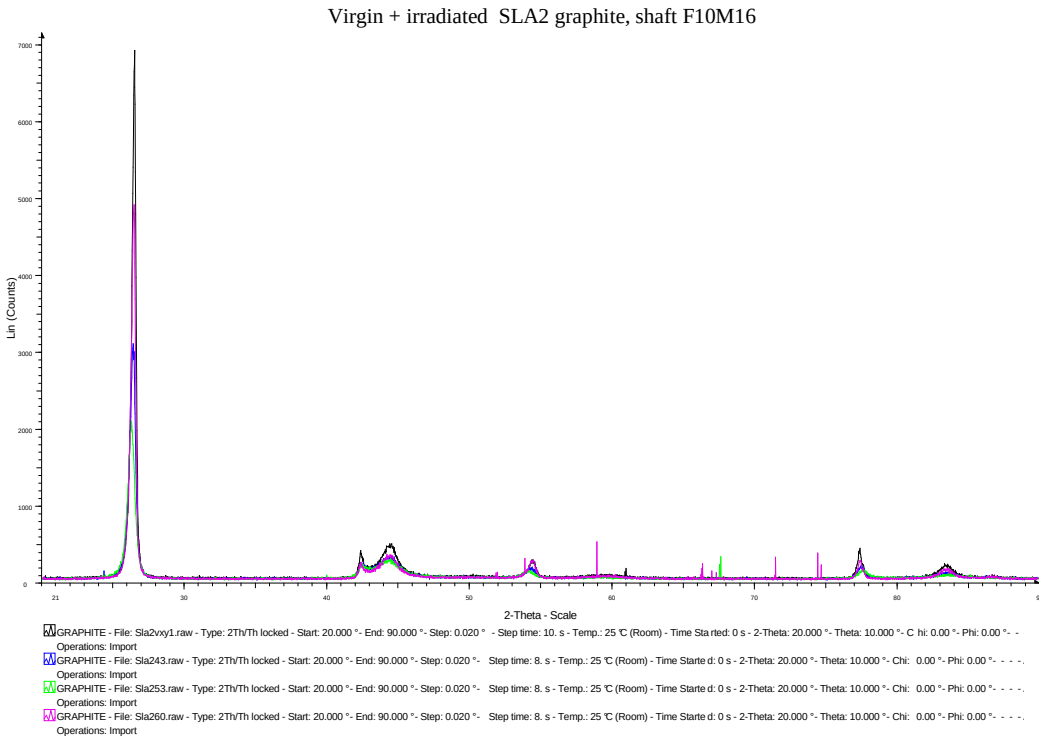

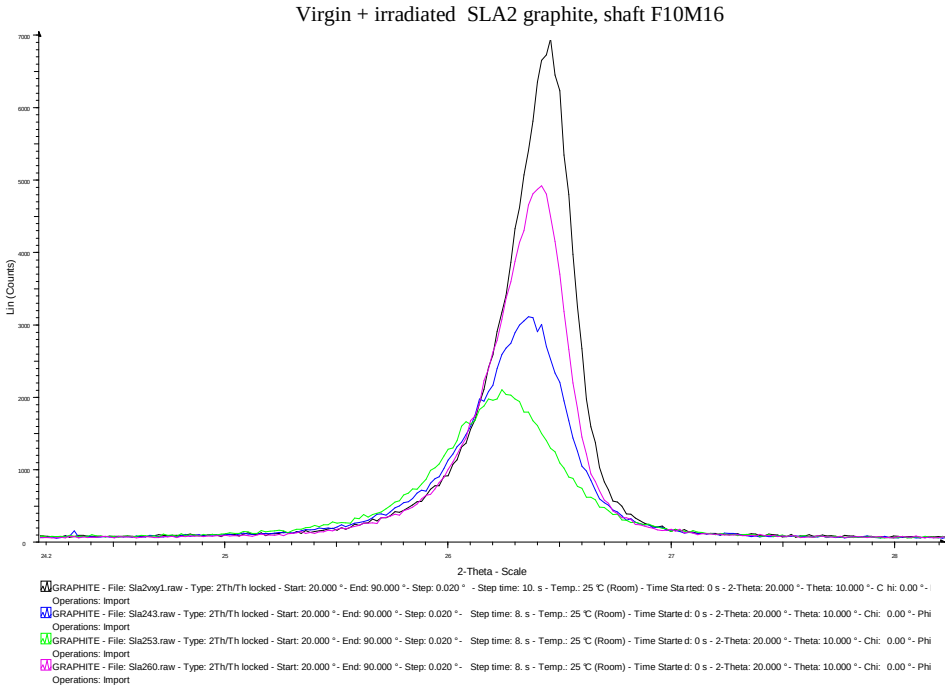

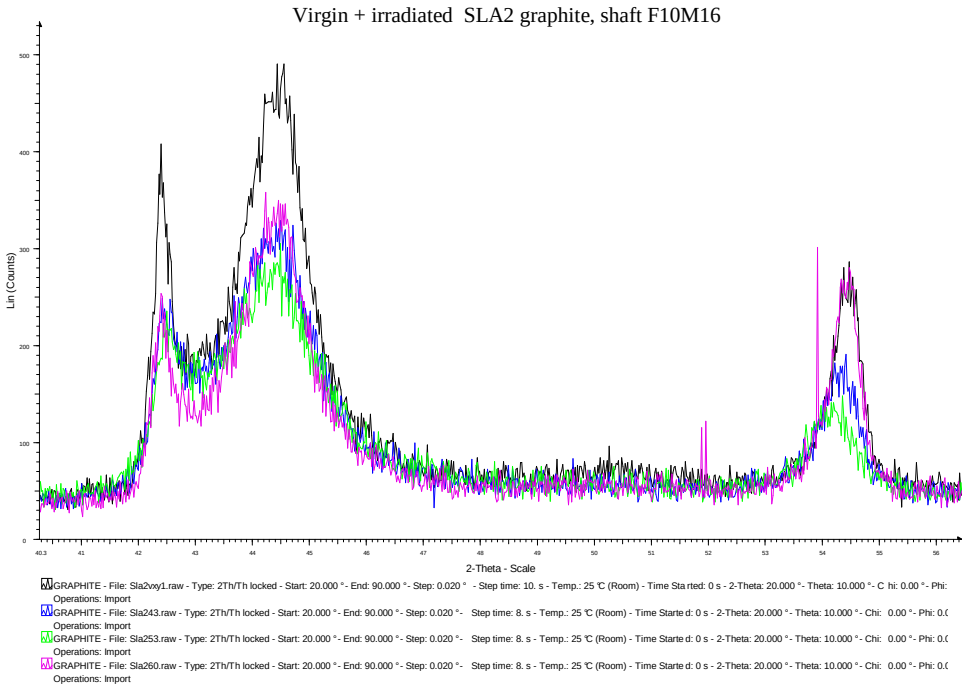

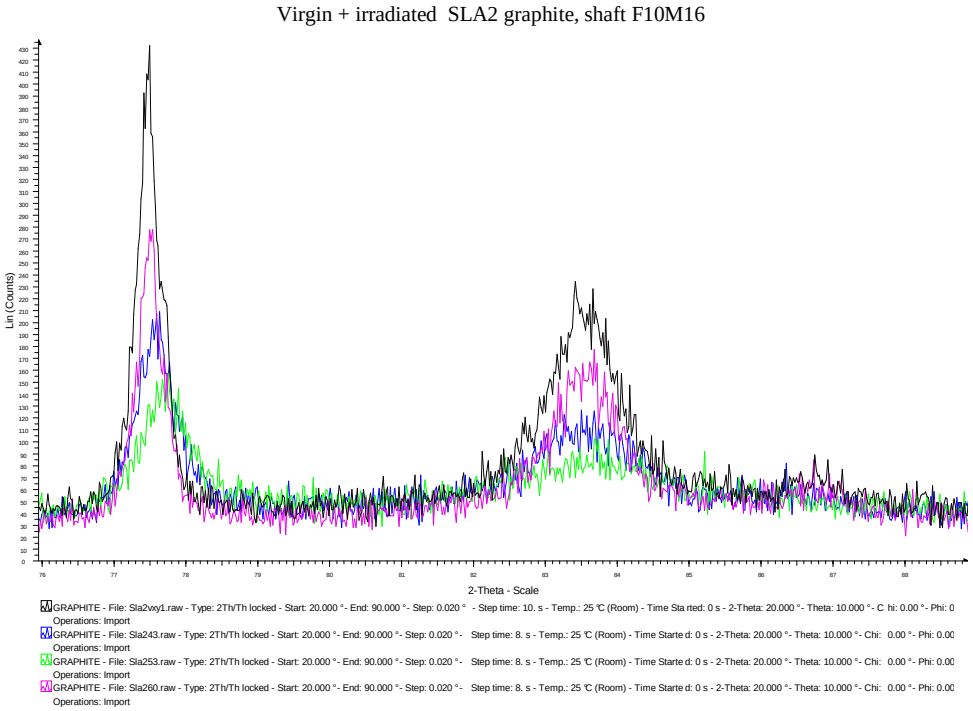

Figure 22: Diffractograms obtained from virgin sample 3784-CD-38869 XY and samples from shaft F10M16 in the SLA2 reactor graphite stack

In this figure, it appears that sample No. 60 displays an odd behaviour compared to what was expected. Since the temperature of irradiation decreases from sample No. 43 (approximately 400°C) to sample No. 60 (approximately 240°C), the latter ought to have the most damaged structure, and therefore the diffractogram should display a wider, less intense line (002) especially shifted farther towards low 2θ values than that of samples Nos. 43 and 53. On the contrary, the diffractogram of sample No. 60 shows a picture of a graphite having only a few defects, as if it had only been weakly irradiated, or at sufficiently high temperatures to anneal a large part of the defects. It should be emphasized that already during the geometric density measurements, this sample displayed unusual behaviour (denser than the reference graphite). Even if this high density value could be explained in some other way, in view of the X-ray diffraction results obtained on this sample and the doubts that hang over its actual provenance within the SLA2 stack, it seems more reasonable to exclude it from comparative analyses with the other irradiated or virgin samples.

With regard to samples Nos. 43 and 53, just as for the irradiated samples of shaft F7M15 whose diffractograms are shown in **Figure 23**, the variations in position of the diffraction lines are in agreement with the existing data, namely the lower the temperature of irradiation, the greater the increase in parameter *c*, the variation in parameter *a* being less marked.

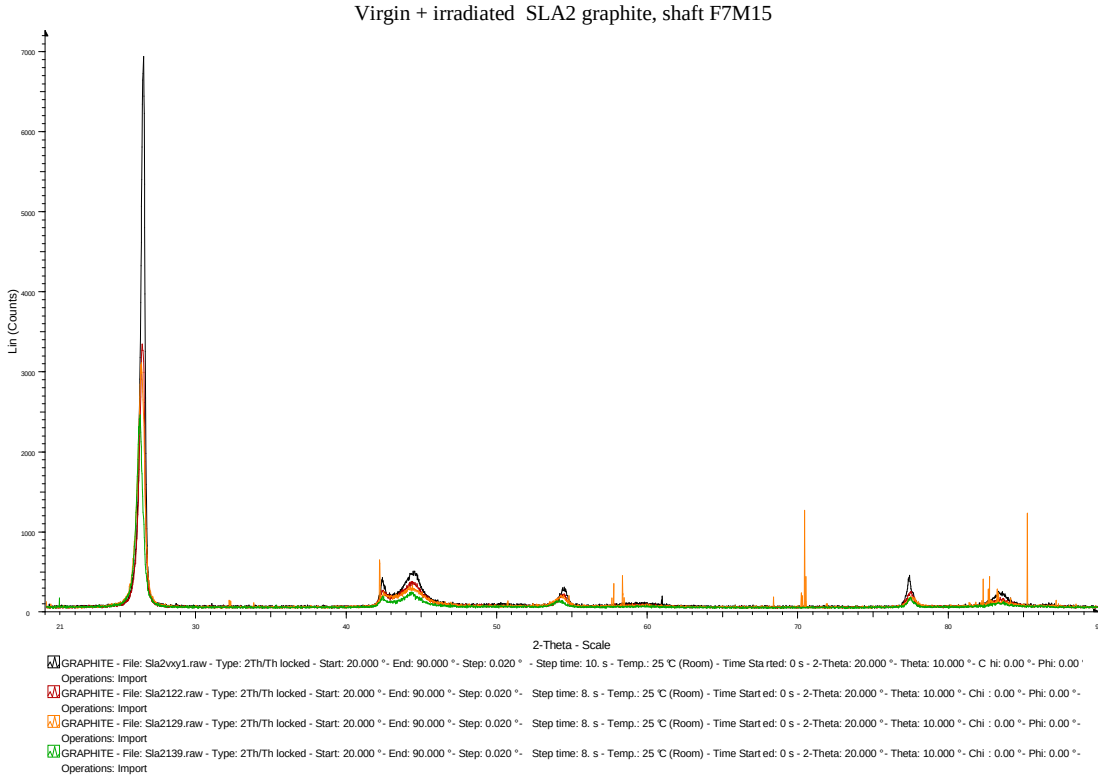

Virgin + irradiated SLA2 graphite, shaft F7M15

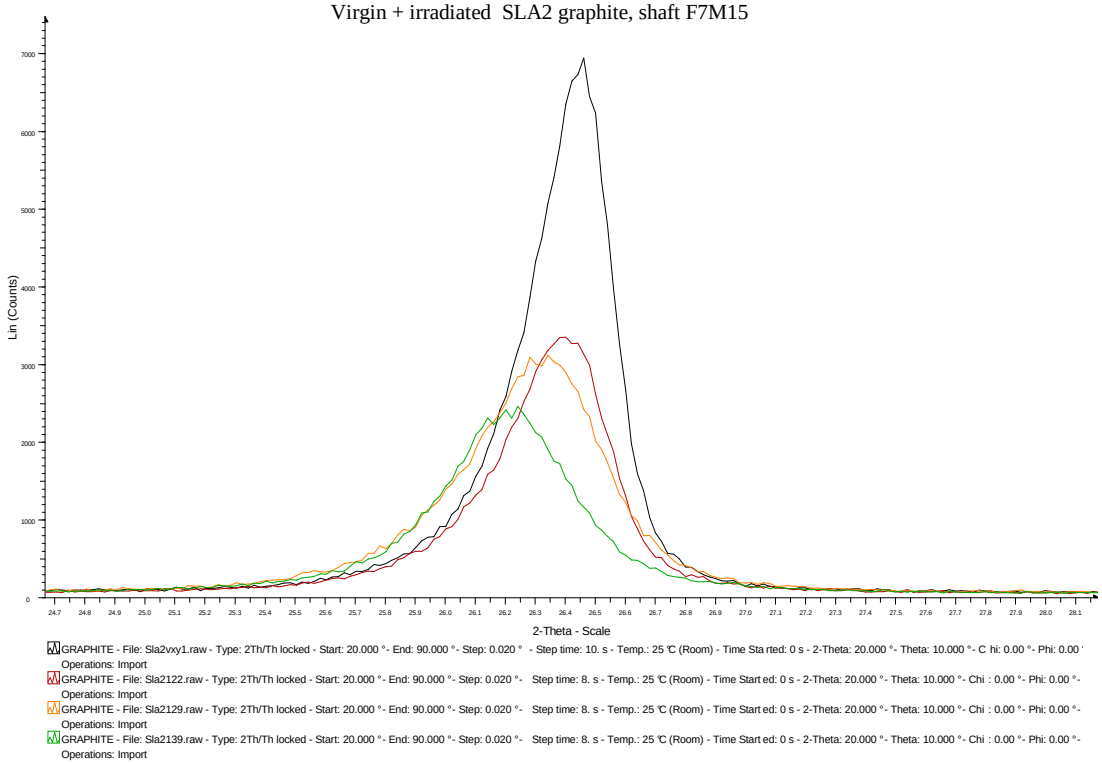

Virgin + irradiated SLA2 graphite, shaft F7M15

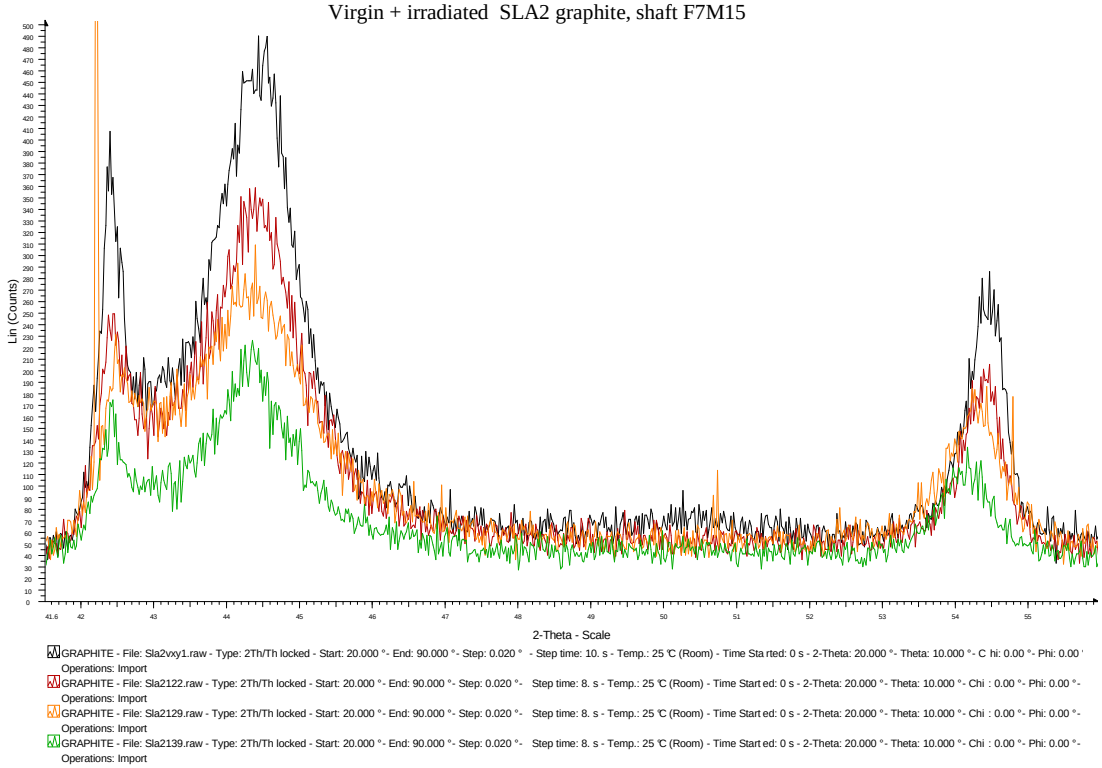

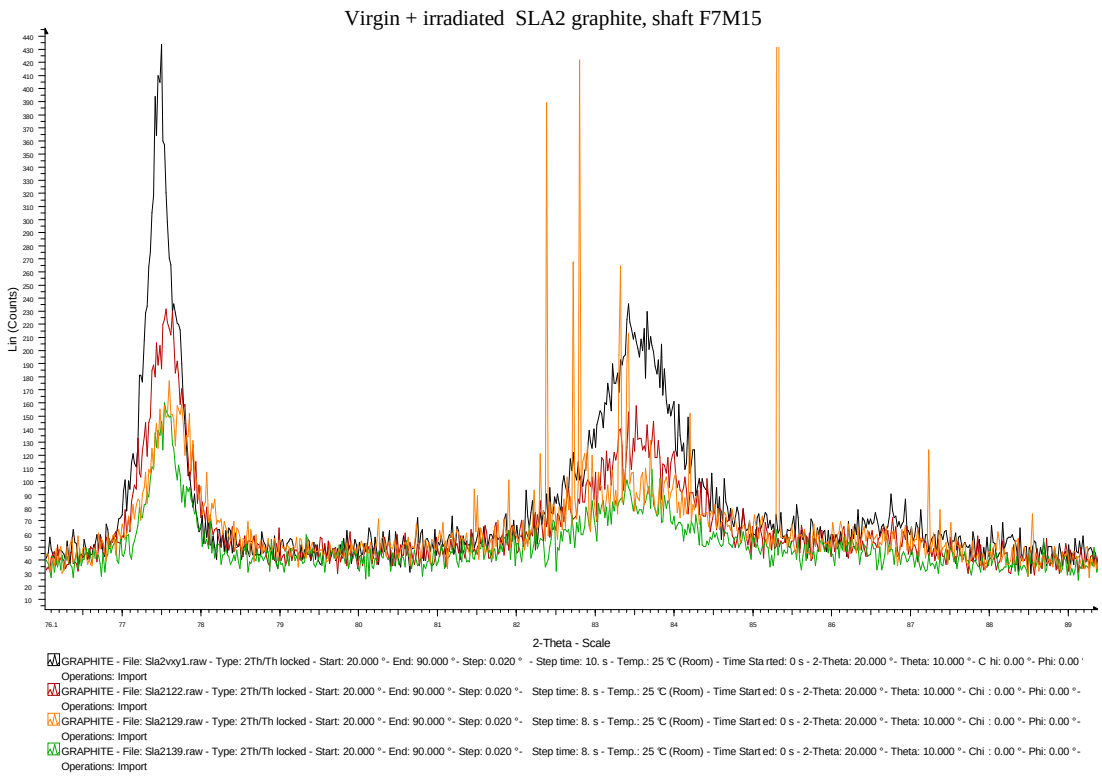

Figure 23: Diffractograms obtained from virgin sample 3784-CD-38869 XY and samples from shaft F7M15 in the SLA2 reactor graphite stack.

Analysis of the recorded diffractograms confirms these initial observations and leads to the lattice parameters shown in **Table 16**.

SLA2	*Tirr (°C)*	*Parameter c*	*Δc/c (%)*	*Parameter a*	*Δa/a (%)*
Theoretical parameters	*NA*	*6.707*	*NA*	*2.461*	*NA*
Non-irradiated reference (3784-CD-38869 XY)	NA	6.740 +/- 0.002	NA	2.462 +/- 0.002	NA
SLA2-43	402	6.755 +/- 0.002	0.28 +/- 0.06	2.457 +/- 0.002	-0.13 +/- 0.16
SLA2-53	288	6.779 +/- 0.002	0.64 +/- 0.06	2.454 +/- 0.002	-0.26 +/- 0.16
SLA2-60	236	6.743 +/- 0.002	0.10 +/- 0.06	2.461 +/- 0.002	0.02 +/- 0.16
SLA2-122	412	6.746 +/- 0.002	0.15 +/- 0.06	2.458 +/- 0.002	-0.09 +/- 0.16
SLA2-129	337	6.762 +/- 0.002	0.38 +/- 0.06	2.456 +/- 0.002	-0.18 +/- 0.16
SLA2-139	236	6.782 +/- 0.002	0.69 +/- 0.06	2.459 +/- 0.002	-0.03 +/- 0.16

Table 16: Crystal parameters of irradiated samples from the SLA2 stack.

Shaft F7M15 being the closest to the centre of the core, it was probably subjected to a slightly higher neutron fluence than that of shaft F10M16. However, since the samples from shafts F10M16 and F7M15 were not taken at the same elevations (except for samples Nos. 60 and 139, but sample No. 60 has been discarded from the analysis), it is not possible to compare the results for these two shafts for studying the possible role of neutron fluence.

Analysis of the diffractograms of the SLA2 irradiated samples has also led to the diffraction line widths (002), (004) and (110) depicted in **Tables 17** and **18** and in **Figure 24**.

Line	*Reference XY (FWHM)*	*SLA2-43*		*SLA2-53*		*SLA2-60*	
		FWHM	*ΔFWHM %*	*FWHM*	*ΔFWHM %*	*FWHM*	*ΔFWHM %*
(002)	0.31	0.452	***47.71***	0.543	***77.45***	0.353	***15.36***
(101)	1.278	1.793	***40.30***	1.919	***50.16***	1.467	***14.79***
(004)	0.602	0.941	***56.31***	1.028	***70.76***	0.67	***11.30***
(110)	0.371	0.635	***71.16***	0.811	***118.60***	0.399	***7.55***

Table 17: Diffraction line mid-height width of the samples from shaft F10M16-C20 of the SLA2 stack.

Line	*Reference XY (FWHM)*	*SLA2-122*		*SLA2-129*		*SLA2-139*	
		FWHM	*ΔFWHM %*	*FWHM*	*ΔFWHM %*	*FWHM*	*ΔFWHM %*
(002)	0.31	0.397	***29.74***	0.512	***67.32***	0.492	***60.78***
(101)	1.278	1.54	***20.50***	1.648	***28.95***	1.653	***29.34***
(004)	0.602	0.653	***8.47***	0.896	***48.84***	0.999	***65.95***
(110)	0.371	0.543	***46.36***	0.655	***76.55***	0.645	***73.85***

Table 18: Diffraction line mid-height width of the samples from shaft F7M15-C19 of the SLA2 stack.

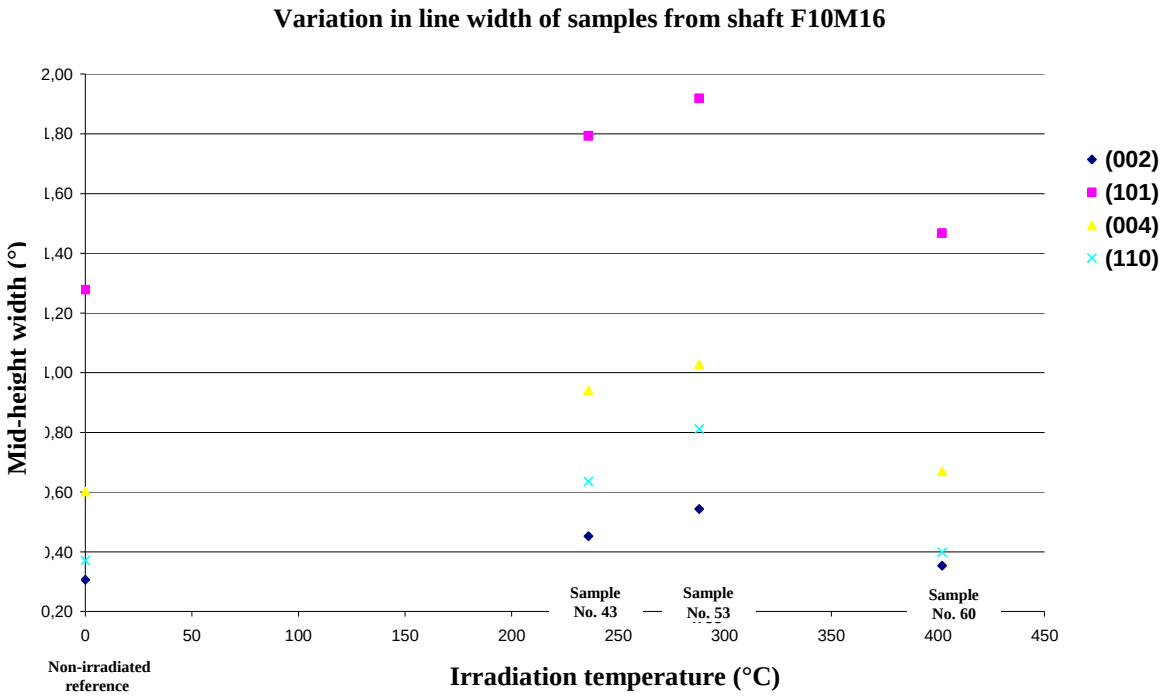

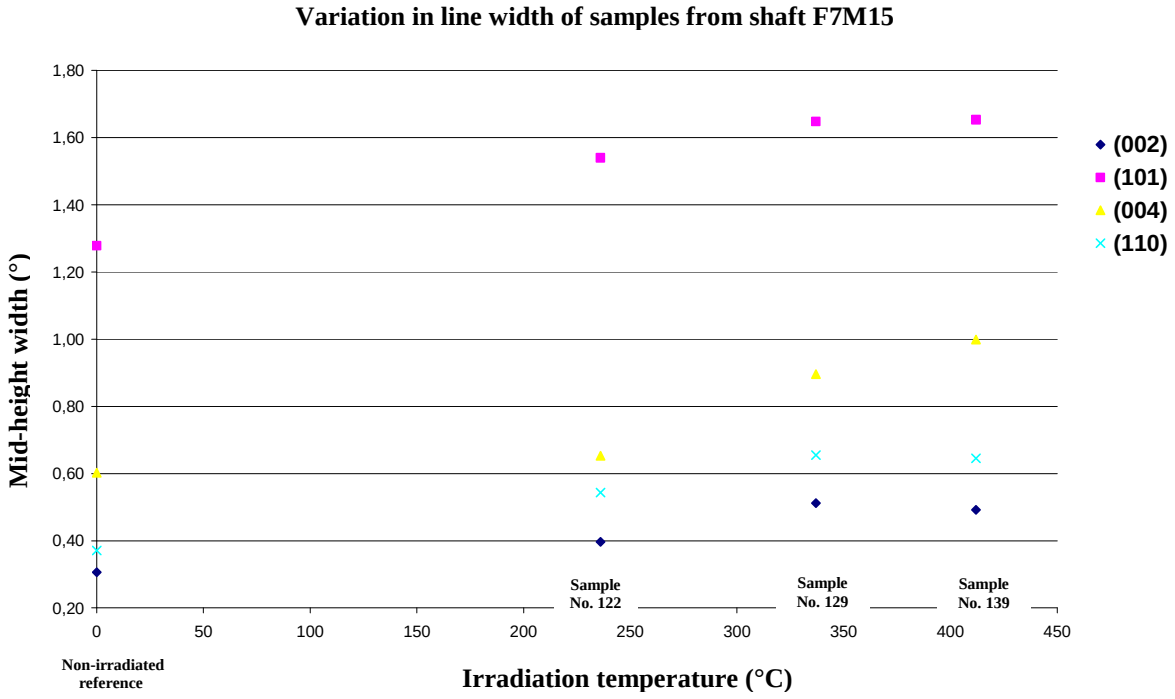

Figure 24: Variation in line width of the samples from shaft F10M16 and F7M15 of the SLA2 reactor graphite stack.

In a diffractogram, diffraction line widening has three origins (11), an instrumental one (H_0, common to all the samples), one associated with the size of the diffracting crystallites / grains (H_l) and a last one (H_g) which is linked to the presence of microdeformations within the crystallites (presence of defects). It should be noted that the last two contributions to modifying diffraction line widths may be modified by neutron irradiation.

$$H = H_0 + H_l + H_g \tag{11}$$

In fact, the H_g term increases with the level of crystal defects (hence a widening of the diffraction lines), a level itself dependent on the neutron fluence and the temperature of irradiation. In addition, studies have shown that graphite crystallites may grow in the *c* direction under irradiation **(Figure 25) [10]**, which leads to a decrease in the H_l factor, and therefore a thinning of the lines in question. Since these two phenomena act at the same time, and the only piece of data available is the overall variation in diffraction line width, the two effects cannot be decorrelated.

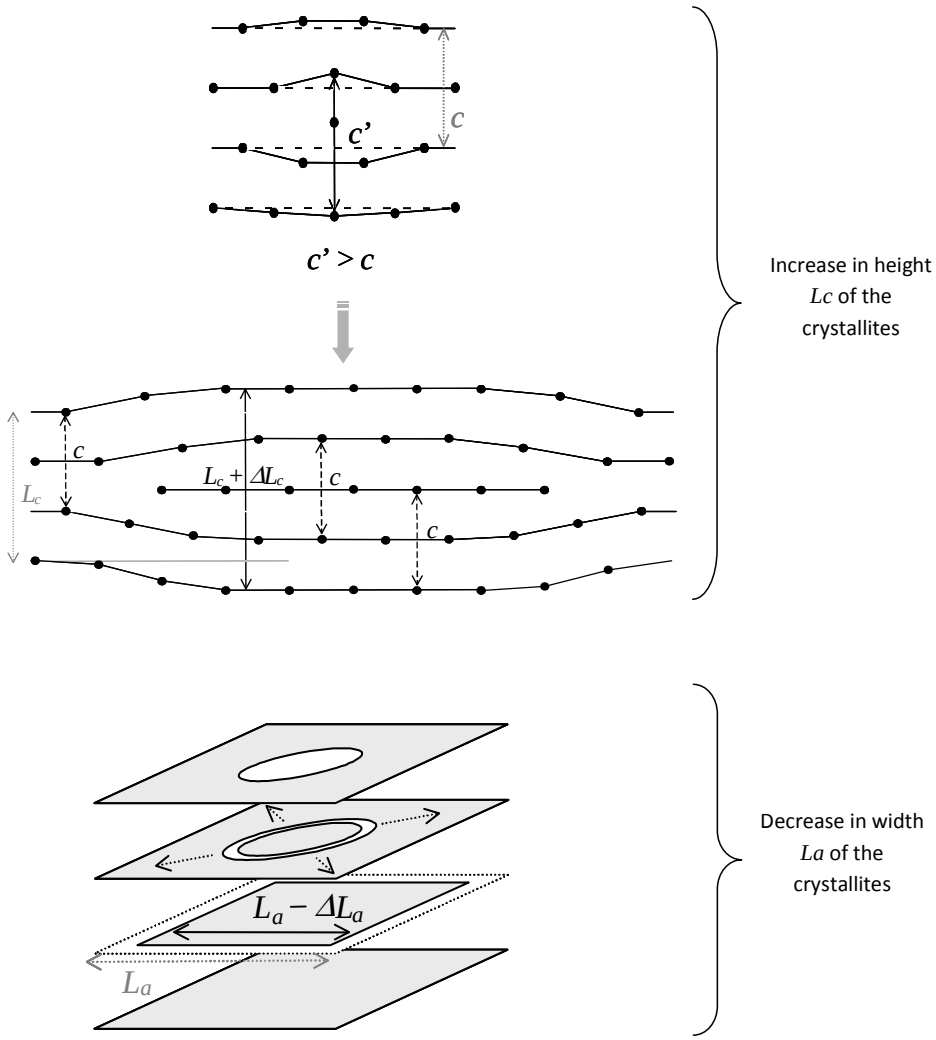

Figure 25: Schematic representation of the height and width of graphite crystallites under irradiation.

Following the results obtained, it appears that the diffraction lines of the irradiated samples from the SLA2 stack all widen, and the lower the temperature of irradiation the more they do so (only sample No. 60 behaves differently, but it has been previously excluded from the analysis). This result is an expression of the fact that the contribution of microdeformations (associated with the concentration of defects: H_g) to diffraction line widening is greater and conceals the contribution of "slimming" (H_l) of the diffraction lines (002) and (004) associated with graphite crystallite growth in the *c* direction.

Thus, since this variation in diffraction line widths is mostly an expression of the concentration of crystal defects in the graphite, the results in **Table 16** are consistent with the relative position of the samples in the SLA2 stack and confirm the results obtained with the crystal parameters, namely the presence of a gradient in microstructural properties (on the crystalline scale) from the bottom to the top of the stack. These results also imply that in the case of crystalline properties, and in contrast to the variation in densities (see paragraphs 6.1 and 6.2), the predominant environmental parameter is the temperature of irradiation (the greater it is, the more there is an annealing of defects) and not neutron fluence.

7. CONCLUSIONS

As part of the studies into the storage of "graphite" waste originating from the UNGG reactor series, it is particularly necessary to obtain scientific data on the behaviour of the long-lived radionuclides ^{36}Cl and ^{14}C given their mobility in the geological medium and their long radioactive period. To do this, an R&D programme was suggested for studying and quantifying the release mechanisms of these radionuclides in water, as well as for studying the variation in the microstructure of graphite under irradiation. This is because the characteristics of the graphite porous medium are essential parameters which will broadly influence the physical and chemical processes that control the release of radionuclides in solution.

With this in mind, samples from the Saint-Laurent A2 reactor have been characterized at the *Laboratoire de caractérisations Physico-Chimiques des Matériaux Irradiés* (Laboratory for Physical and Chemical Characterization of Irradiated Materials) (DMN/SEMI/LPCMI) and at the *Laboratoire d'Analyses Chimiques et Radiochimiques* (Laboratory for Chemical and Radiochemical Analyses) (DEC/SA3C/LARC) with the support of the *Laboratoire d'Expertise et de Caractérisation Destructive* (Specialist Laboratory in Destructive Characterization) (DSN/SEEC/LECD). These characterizations mainly focused on density measurements, porosimetry and X-ray diffraction, the Raman characterizations initially planned having been postponed to the second half of 2010 (ATALANTE − CEA Marcoule).

As a result of the characterization of the representative virgin samples from the SLA2 reactor stack, the geometric and hydrostatic density results were found to be quite consistent between the various laboratories with an average value of 1.69 ± 0.02 for a value drawn from data in the literature of 1.68 **[6]**. Total porosity is estimated at 25.7% and is mostly due to open porosity

(approximately 21%), closed porosity remaining relatively low with a value of about 5%. Mercury porosimetry tests on virgin samples are currently in progress.

Twelve irradiated samples originating from different elevations within shafts F10M16 and F7M15 were also characterized, 6 at DMN/SEMI/LPCMI and 6 at DEC/SA3C/LARC. Generally speaking, irradiation led to quite a small change in the characteristics of the graphite, the average wear being less than 5%, although it reaches values close to 8% locally. Overall, a decrease in density is found, associated with an increase in open porosity, but in contrast with the graphite of the G2 reactor stack, without any particularly distinct variation in closed porosity. This decrease in density is associated with the radiolytic corrosion of graphite, corrosion which is all the greater when the samples are subject to high fluences and irradiation temperatures. Thus, the density, the percentages of total and open porosity, and thereby the degree of wear of the graphite are modelled on the fluence profile of the Saint-Laurent A2 reactor. There does appear, however, a more worn zone between elevations 1 500 mm and 2 000 mm from the bottom of the graphite stack. This particular wear could be explained as the local result of a high temperature of irradiation associated with a neutron fluence still sufficiently intense to produce a large quantity of radical species O*, species causing radiolytic corrosion. It is also important to stress that the results obtained generally agree with those arising from a previous study **[5]**, which now provides a large amount of significant experimental data on the irradiated graphite of the SLA2 reactor stack.

LIST OF TABLES

LIST OF FIGURES

REFERENCES

[1] *"Caractérisation des graphites des empilements G2 avant et après irradiation " (Characterization of G2 stack graphites before and after radiation),* J. COMTE, L. GOSMAIN, Ch. GUY
Technical report DEC/SA3C/LARC – 09/008, December 2009

[2] *"Réacteurs à uranium naturel graphite-gaz " (Uranium Natural Graphite-Gas reactors),* D. BASTIEN
Engineering techniques, B 3180, 1993

[3] *"Caractérisations mécanique, chimique et radiologique du graphite des réacteurs de la filière UNGG" (Mechanical, chemical and radiological characterizations of UNGG reactor type graphite),* I. BRESARD, J.P. BONAL
CEA, Nuclear Energy Division, Scientific and technical article, 2000 Edition

[4] *"212ème bulletin de santé de la famille UNGG – 2ème trimestre 1980" (212th Health Bulletin of the UNGG family − 2nd quarter of 1980),* D. BASTIEN
DEDR/CRG/80-147/DB/MCM, 31 July 1980

[5] *"Caractérisation du graphite de Saint-Laurent A2 " (Characterization of Saint-Laurent A2 graphite),* J.P. BONAL, L.MOITRELLE, D.CURY, Ph. MONGABURE
Technical report DMN/SEMI/LM2E – 2006-021/A, November 2006

[6] *"Caractéristiques du graphite de l'empilement de SL2. Regroupement des caractéristiques des graphites des réacteurs G1, G2, G3, EDF1, EDF2, EDF3, EDF4" (Characteristics of SL2 stack graphite. Compilation of the graphite characteristics of the G1, G2, G3, EDF1, EDF2, EDF3, EDF4 reactors),* M. YVARS, M.T. GAUDEZ
Technical reports DPC/PCA/SPMN 68-60, March 1968

[7] *"Texture poreuse de nouveaux type de graphites" (Porous texture of new types of graphites),* M. YVARS,
Technical reports DPC/PCA/SPMN 67-28, March 1967

[8] *"Graphite des empilements des réacteurs UNGG:Chinon A3,Bugey 1,Saint Laurent A2. Synthèse des mesures des propriétés mécaniques et de dégazage –état d'avancement 2006" (Graphite of UNGG reactor stacks: Chinon A3, Bugey 1, Saint Laurent A2. Summary of Measurements of Mechanical Properties and Degasification − State of Progress 2006),* S. PARRAUD
Technical report CEA/CAD/DGI/SEEC/LECD R3 NT352

[9] *"Le graphite dans les réacteurs à haute température 2ème partie: le comportement du graphite sous irradiation" (Graphite in high temperature reactors 2nd Part: behaviour of graphite under irradiation),* L. GOSMAIN, J.P. BONAL
Technical report DMN/SEMI/LM2E 03-045/B, January 2005

[10] *"Dimensional changes in the irradiated graphite lattice",* P.R. GOGGIN, R.W. HENSON, A.J. PERKS, W.N. REYNOLDS
Carbon, Vol.1, p189-200, 1964

[11] *"Irradiation damage in graphite due to fast neutrons in fission and fusion systems "*
IAEA – TECDOC – 1154, April 2000

APPENDIX 1: ICDD data sheet for graphite

Pattern : 00-025-0284 *Radiation =* 1.540598 *Quality :* Deleted

C

Carbon
Graphite, syn

Lattice : Hexagonal *Mol. weight =* 12.01

S.G. : P63/mmc (194) *Volume [CD] =* 34.98

a = 2.45600 *Dx =* 2.281

c = 6.69600

Z = 4

Deleted Or Rejected By. Deleted by 00-041-1487; good experiment pattern; Bayliss 6/90. Unit Cell Data Source: Powder Diffraction. Data collection flag: Ambient.

Holcombe, USAEC Oak Ridge Y-12 Plant, Report Y1887 (1973)., Private Communication (1974)

CAS Number: 7440-44-0

Radiation : CuKα *Filter :*

Lambda : 1.54178 *d-sp :* Calculated spacings

SS/FOM : F19=269(0.0020,24)

2th	i	h	k	l
26.603	100	0	0	2
42.465	3	1	0	0
44.670	15	1	0	1
50.825	3	1	0	2
54.794	6	0	0	4
60.034	4	1	0	3
71.691	1	1	0	4
77.699	4	1	1	0
83.847	6	1	1	2
85.640	1	1	0	5
87.297	1	0	0	6
94.346	1	2	0	1
102.142	4	1	1	4
106.703	1	2	0	3
124.004	1	1	0	7
133.943	1	0	0	8
135.322	1	2	0	5
137.712	4	1	1	6
149.613	2	2	1	1